

AD-A134 378

CHAIN REACTION MECHANISM FOR I2 DISSOCIATION IN THE 02  
(1 DELTA)-I ATOM L. (U) AEROSPACE CORP EL SEGUNDO CA  
AEROPHYSICS LAB. R F HEIDNER ET AL. 20 SEP 83

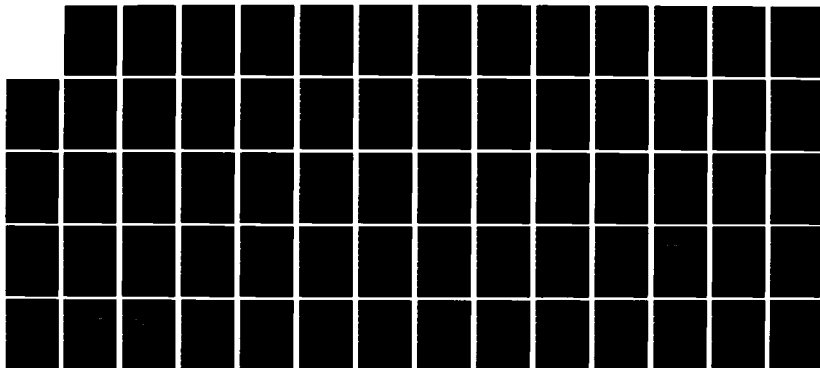
1/1

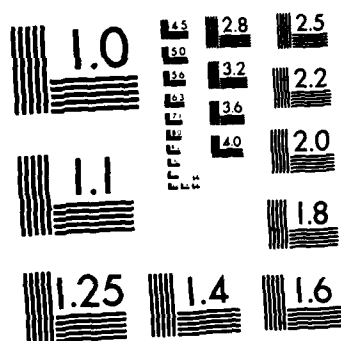
UNCLASSIFIED

TR-0083(3610)-1 SD-TR-83-60

F/G 7/4

NL





MICROCOPY RESOLUTION TEST CHART  
NATIONAL BUREAU OF STANDARDS-1963-A

AD-A134 370

12

Chain Reaction Mechanism for  $I_2$  Dissociation  
in the  $O_2 (^1\Delta)$ -I Atom Laser

R. F. HEIDNER III, C. E. GARDNER,  
G. I. SEGAL, and T. M. EL-SAYED  
Aerophysics Laboratory  
The Aerospace Corporation  
El Segundo, Calif. 90245

20 September 1983

APPROVED FOR PUBLIC RELEASE;  
DISTRIBUTION UNLIMITED

DTIC  
ELECTE  
NOV 1 1983  
A

DTIC FILE COPY

Prepared for  
SPACE DIVISION  
AIR FORCE SYSTEMS COMMAND  
Los Angeles Air Force Station  
P.O. Box 92960, Worldway Postal Center  
Los Angeles, Calif. 90009

507

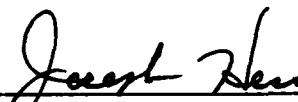
This report was submitted by The Aerospace Corporation, El Segundo, CA 90245, under Contract No. F04701-82-C-0083 with the Space Division, Deputy for Technology, P.O. Box 92960, Worldway Postal Center, Los Angeles, CA 90009. It was reviewed and approved for The Aerospace Corporation by W. P. Thompson, Director, Aerophysics Laboratory. 1st Lt Steven G. Webb, AFSTC, WCO, was the Air Force project officer.

This report has been reviewed by the Public Affairs Office (PAS) and is releasable to the National Technical Information Service (NTIS). At NTIS, it will be available to the general public, including foreign nationals.

This technical report has been reviewed and is approved for publication. Publication of this report does not constitute Air Force approval of the report's findings or conclusions. It is published only for the exchange and stimulation of ideas.



Steven G. Webb, 1st Lt, USAF  
Project Officer



Joseph Hess, GM-15, Director  
West Coast Office, AF Space Technology  
Center

UNCLASSIFIED

SECURITY CLASSIFICATION OF THIS PAGE (When Data Entered)

REPORT DOCUMENTATION PAGE		READ INSTRUCTIONS BEFORE COMPLETING FORM
1. REPORT NUMBER SD-TR-83-60	2. GOVT ACCESSION NO. <b>A134370</b>	3. RECIPIENT'S CATALOG NUMBER
4. TITLE (and Subtitle) CHAIN REACTION MECHANISM FOR $I_2$ DISSOCIATION IN THE $O_2(^1\Delta)$ - I ATOM LASER		5. TYPE OF REPORT & PERIOD COVERED
7. AUTHOR(s) R. F. Heidner III, C. E. Gardner, G. I. Segal and T. M. El-Sayed		6. PERFORMING ORG. REPORT NUMBER TR-0083(3610)-1
9. PERFORMING ORGANIZATION NAME AND ADDRESS The Aerospace Corporation El Segundo, Calif. 90245		8. CONTRACT OR GRANT NUMBER(s) F04701-82-C-0083
11. CONTROLLING OFFICE NAME AND ADDRESS Space Division Air Force Systems Command Los Angeles, Calif. 90009		10. PROGRAM ELEMENT, PROJECT, TASK AREA & WORK UNIT NUMBERS
14. MONITORING AGENCY NAME & ADDRESS (if different from Controlling Office)		12. REPORT DATE 20 September 1983
		13. NUMBER OF PAGES 62
		15. SECURITY CLASS. (of this report) Unclassified
		15a. DECLASSIFICATION DOWNGRADING SCHEDULE
16. DISTRIBUTION STATEMENT (of this Report)  Approved for public release; distribution unlimited		
17. DISTRIBUTION STATEMENT (of the abstract entered in Block 20, if different from Report)		
18. SUPPLEMENTARY NOTES		
19. KEY WORDS (Continue on reverse side if necessary and identify by block number) <div style="display: flex; justify-content: space-between;"> <div>           Chemical Kinetics            Computerized Data Acquisition            Electronic Excitation            Emission Spectroscopy         </div> <div>           Energy Transfer            Iodine            Kinetic Flow Tube            Lasers (cw)         </div> <div>           Oxygen         </div> </div>		
20. ABSTRACT (Continue on reverse side if necessary and identify by block number) <p>A chain reaction model for <math>I_2</math> dissociation in <math>O_2^*</math> is proposed. Experiments in a computer-controlled flow tube apparatus indicate that <math>I_2(X)</math> dissociation is initiated by collisions with <math>O_2(^1I)</math>; subsequently, the I atoms formed are pumped to <math>I^*</math> by <math>O_2(^1\Delta)</math>. Other initiation mechanisms are also discussed. Chain branching occurs when <math>I^*</math> transfers energy to <math>I_2(X)</math> to form <math>I_2^*</math> and <math>I_2^*</math> is dissociated into I atoms by collisions with <math>O_2(^1\Delta)</math>. Chain termination in these experiments is caused by I-atom wall recombination. An analytic model</p>		

DD FORM 1473  
(FACSIMILE)

UNCLASSIFIED

SECURITY CLASSIFICATION OF THIS PAGE (When Data Entered)

UNCLASSIFIED

SECURITY CLASSIFICATION OF THIS PAGE(When Data Entered)

19. KEY WORDS (Continued)

20. ABSTRACT (Continued)

is presented that favors the above explanation over several others that are kinetically similar. Numerical modeling calculations are included to verify this simplified model. Scaling relationships are developed for  $I_2(X)$  dissociation as a function of  $[O_2(^1\Delta)]$ ,  $[O_2(^3\Sigma)]$ ,  $[I_2]_0$ ,  $[H_2O]$ , and  $[Ar]$ . The  $I_2$  intermediate ( $I_2^\ddagger$ ) is not directly observed; however, indirect evidence indicates that it is vibrationally excited  $I_2(X)$ .

UNCLASSIFIED

SECURITY CLASSIFICATION OF THIS PAGE(When Data Entered)

## ACKNOWLEDGMENTS

The authors wish to acknowledge the continuing support of and interest in this work by Lt. Col. W. E. McDermott and the staff members of the New Laser Concepts Branch of the Air Force Weapons Laboratory. The active participation of Prof. J. V. V. Kasper was crucial to the early stages of this program. One of us (RFH) would like to acknowledge the invaluable exchange of ideas with many colleagues working actively in this field. These include Drs. H. Lilienfeld (McDonnell Douglas), A. T. Pritt, Jr. and D. Benard (Rockwell Science Center), G. Fisk and G. Hays (Sandia), J. Berg (TRW), G. Black (SRI), and Profs. P. L. Houston and J. R. Wiesenfeld (Cornell University). We wish to thank H. Michels (UTRC) and Prof. J. Tellinghuisen (Vanderbilt University), and J. B. Koffend (Lyon) for recent information regarding potential energy curve calculations and spectroscopy of the  $A'^3\Pi_{2u}$  state of  $I_2$ . Many thanks are due to Mrs. Karen Foster who performed the NEST calculations and Ms. Lydia Hammond who prepared the manuscript.

Accession For  
THIS CASE  
DATE THE  
UNCLASSIFIED

FBI  
FBI  
FBI

FILED

A-1

OFFICE  
OF THE  
DIRECTOR

## CONTENTS

ACKNOWLEDGMENTS.....	1
I. INTRODUCTION.....	9
II. EXPERIMENTAL APPARATUS.....	15
III. ANALYTIC MODELING OF I <sub>2</sub> DISSOCIATION.....	21
A. Steady-State O <sub>2</sub> ( <sup>1</sup> Σ) + I <sub>2</sub> Model.....	24
B. Sequential Model with I <sub>2</sub> <sup>‡</sup> in Steady State.....	25
C. Global Analytic Equation.....	26
IV. RESULTS AND DISCUSSION.....	29
A. Initiation Effects and Induction Times.....	29
B. Extent of I <sub>2</sub> Dissociation in Steady State.....	36
C. I <sub>2</sub> Dissociation Half-Life and Extent of Dissociation: Variation with Initial Conditions (Table 3).....	36
D. Behavior of I <sub>2</sub> (A <sup>3</sup> Π <sub>1u</sub> ) and I <sub>2</sub> (B <sup>3</sup> Π <sub>0u</sub> <sup>+</sup> ).....	52
E. I <sub>2</sub> Dissociation in an H <sub>2</sub> O-Free O <sub>2</sub> <sup>*</sup> System.....	55
V. SUMMARY AND CONCLUSIONS.....	61
REFERENCES.....	63
APPENDIX A - DEFINITIONS FOR ANALYTIC MODELING.....	65
APPENDIX B - ANALYTIC DISSOCIATION MODEL FOR I <sub>2</sub> INCLUDING I ATOM RECOMBINATION.....	67



## FIGURES

1.	Low-Lying Electronic Energy Levels for the $O_2$ and $I_2$ Molecules and the I Atom.....	10
2.	Schematic Diagram of the Computer-Controlled Kinetic Flow Tube Apparatus.....	16
3.	Low Resolution Spectrum of the $I_2(A_2 + X)$ Transition Underlying the Spectrum of $O_2(^1\Delta + ^3\Sigma)$ and $I(^2P_{1/2} + ^2P_{3/2})$ .....	18
4.	Mixing Efficiency of $I_2(+Ar)$ into $O_2$ Using the Radial Injector (Fig. 2): $O-I_2 + Ar$ Mixture from the Saturator; $\Delta$ - Additional Pure Ar Injected with $I_2 + Ar$ Mix.....	19
5.	Effect of $O(^3P)$ on Dissociation Initiation.....	30
6.	$I_2$ Dissociation by Means of the $^1\Sigma + I_2$ Mechanism.....	32
7.	Experimental Data [Table 3: Runs A1(O), A3( $\Delta$ ), and A5(O)], Analytic Model Fits (-), and Numerical Model Fits (---) for $I_2$ Dissociation Versus Time as a Function of $[^1\Delta]_0$ .....	37
8.	Plots of $\log t_{1/2}$ Versus $\log [^1\Delta]_0$ .....	38
9.	Experimental Data [Table 3: Runs B1(O), B3( $\Delta$ ), and B5(O)], Analytic Model Fits (-), and Numerical Model Fits (---) for $I_2$ Dissociation Versus Time as a Function of $[^3\Sigma]_0$ .....	41
10.	Plots of $\log t_{1/2}$ Versus $\log [^3\Sigma]_0$ .....	42
11.	Experimental Data [Table 3: Runs C3(O), C2( $\Delta$ ), and C1(O)], Analytic Model Fits (-), and Numerical Model Fits (---) for $I_2$ Dissociation Versus Time as a Function of $[I_2]_0$ .....	43
12.	Plots of $\log t_{1/2}$ Versus $\log [I_2]_0$ .....	44
13.	Experimental Data [Table 3: Runs D2(O), D4( $\Delta$ ), and D6(O)], Analytic Fits (-), Numerical Fits (---) for $I_2$ Dissociation Versus Time as Function of $[H_2O]$ .....	46
14.	Plots of $\log t_{1/2}$ Versus $\log [H_2O]_0$ .....	47

# FIGURES (Continued)

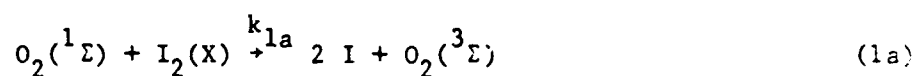
15.	Experimental Data [Table 3: Runs E1(●), E2(□), E3(○); E4(Δ)], Analytic Fit (to Run E1) (-), Numerical Fit (to Run E1) (---) for I <sub>2</sub> Dissociation Versus Time as a Function of [Ar].....	48
16.	Plots of Log t <sub>1/2</sub> Versus Log [Ar].....	49
17.	Time Profiles for I <sub>2</sub> (A → X) and I <sub>2</sub> (B → X) Relative to Other Measured Species.....	53
18a.	I <sub>2</sub> Dissociation in an H <sub>2</sub> O-Free O <sub>2</sub> <sup>*</sup> System: Full Dissociation, Constant [I <sub>2</sub> ] <sub>0</sub> = 2.0 × 10 <sup>13</sup> /cm <sup>3</sup> .....	57
18b.	I <sub>2</sub> Dissociation in an H <sub>2</sub> O-Free O <sub>2</sub> <sup>*</sup> System: Partial Dissociation, Decaying [I <sub>2</sub> ] <sub>0</sub> = 1.3 × 10 <sup>14</sup> /cm <sup>3</sup> .....	58

# TABLES

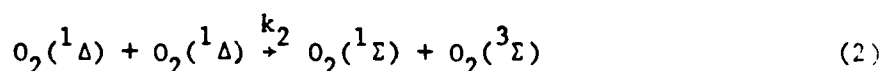
1.	Kinetic Model of $I_2$ Dissociation by $O_2^*$ (T = 295 K).....	23
2.	Analytic Dissociation Model Parameters.....	28
3.	Experimental Conditions and $I_2$ Dissociation Half-Lives.....	33
4.	Maximum Influence of $O_2(^1\Sigma) + I_2$ on $I_2$ Dissociation.....	35
5.	Rate Coefficients for the Chain-Reaction Model.....	40

## I. INTRODUCTION

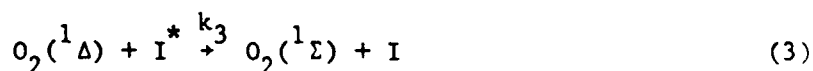
In 1966, Arnold, Finlayson, and Ogryzlo<sup>1</sup> observed that I<sub>2</sub> was rapidly dissociated in the presence of electronically excited oxygen. In addition, strong electronic emission was observed from both molecular I<sub>2</sub> and the product I atoms. These authors noted that O<sub>2</sub>(<sup>1</sup>Σ) (Fig. 1) has sufficient energy to dissociate I<sub>2</sub>(X) by a near-resonant, dissociative E + E energy transfer process:



By means of conventional flow tube techniques, they measured a rapid increase of O<sub>2</sub>(<sup>1</sup>Σ) with time when I<sub>2</sub> was added to the flow. Subsequent work<sup>2-4</sup> has confirmed their hypothesis that O<sub>2</sub>(<sup>1</sup>Σ) is initially formed by Process (2)



and then strongly supplemented by Process (3)



The I\* is produced by the near-resonant E + E exchange process<sup>1,3</sup>

<sup>1</sup>S. J. Arnold, N. Finlayson, and E. A. Ogryzlo, J. Chem. Phys. 44, 2528 (1966).

<sup>2</sup>R. G. Derwent and B. A. Thrush, Trans. Faraday Soc. 67, 2036 (1971).

<sup>3</sup>R. G. Derwent and B. A. Thrush, Disc. Faraday Soc. 53, 162 (1972)

<sup>4</sup>R. F. Heidner III, C. E. Gardner, T. M. El-Sayed, G. I. Segal, and J. V. V. Kasper, J. Chem. Phys. 74, 5618 (1981).

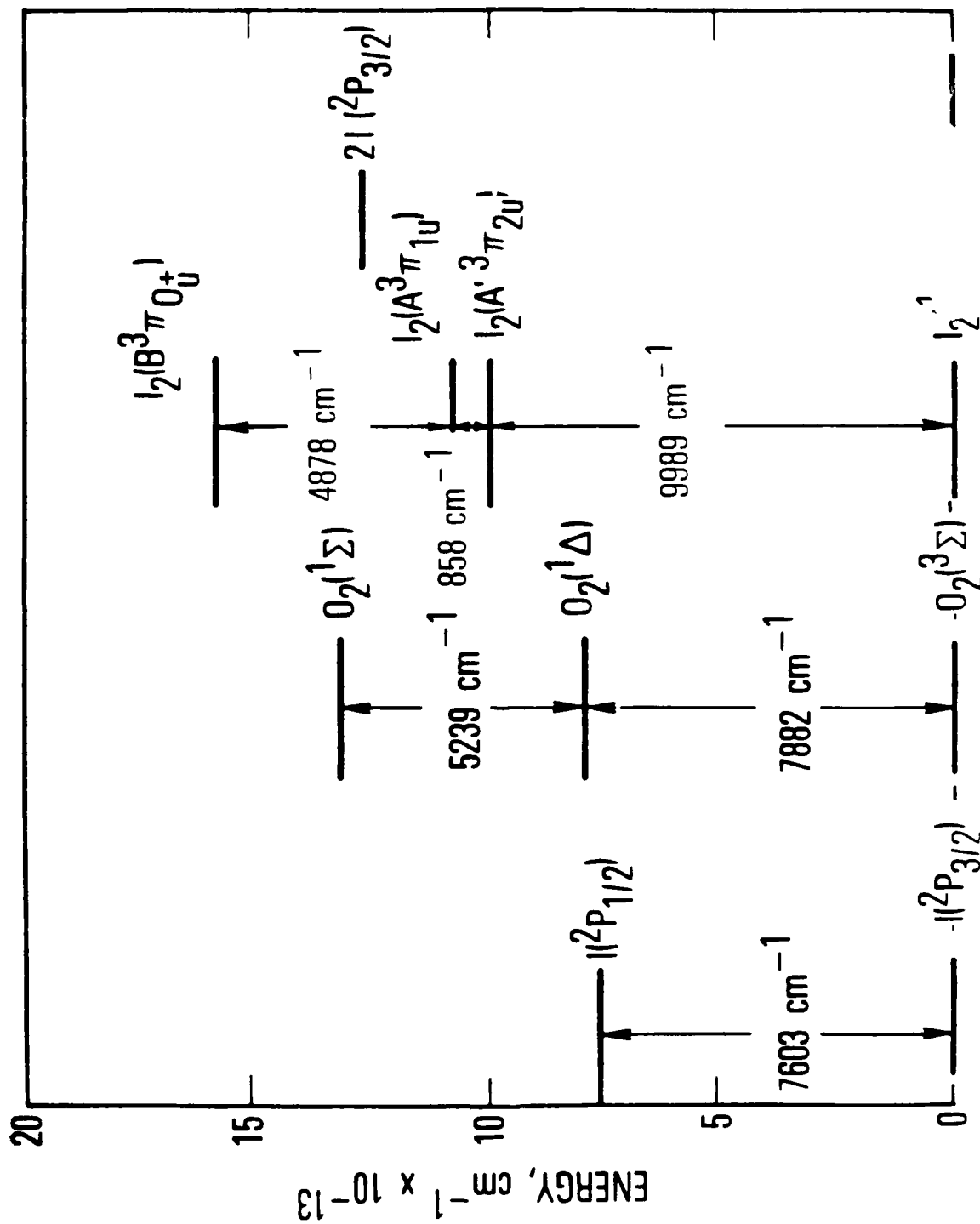
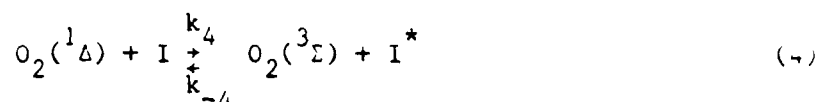
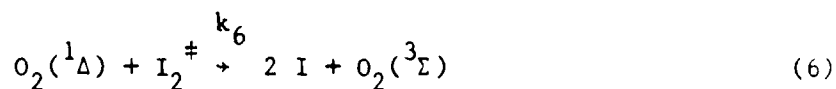
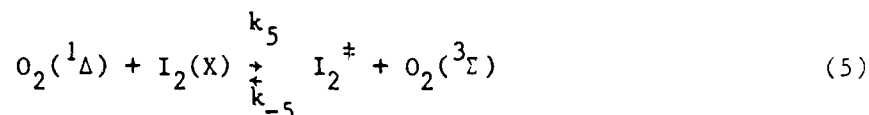


Fig. 1. Low-Lying Electronic Energy Levels for the  $O_2$  and  $I_2$  Molecules and the  $I$  Atom.



where  $K_{\text{EQ}} \equiv k_4/k_{-4} = 2.9$  at  $T = 295$  K.

Arnold et al. suggested a second possibility for  $\text{I}_2$  dissociation: a sequential excitation of  $\text{I}_2(\text{X})$  by consecutive collisions with two  $\text{O}_2(^1\Delta)$  molecules. The  $\text{I}_2$  intermediate suggested was the then unidentified  $\text{A}'^3\pi_{2u}$  state of  $\text{I}_2$ , although these authors noted that calculations for this state generally placed it well above the  $7882 \text{ cm}^{-1}$   $T_0$  value for  $\text{O}_2(^1\Delta)$ :



This brief, but incisive, report still serves as a useful introduction to the subject of  $\text{I}_2$  dissociation in electronically excited oxygen. The recent demonstration of continuous-wave lasing on the  $\text{I}(^2\text{P}_{1/2} \rightarrow ^2\text{P}_{3/2})$  transition<sup>5-7</sup> at  $1.315 \mu\text{m}$  that is pumped by Process (4) gave this kinetic problem new urgency. Clearly, the production of the lasing species (I atoms) must be understood if the potential of this laser system is to be realized.

<sup>5</sup>W. E. McDermott, N. R. Pchelkin, D. J. Benard, and R. R. Bousek, Appl. Phys. Lett. 32, 469 (1978).

<sup>6</sup>D. J. Benard, W. E. McDermott, N. R. Pchelkin, and R. R. Bousek, Appl. Phys. Lett. 34, 40 (1979).

<sup>7</sup>R. J. Richardson and C. E. Wiswall, Appl. Phys. Lett. 35, 138 (1979).

In 1970-72, Derwent and Thrush<sup>2,3,8-10</sup> performed detailed experiments on the  $O_2-I_2$  system to quantify the observations of Arnold et al. Much of their analysis has proven correct; however, they concluded<sup>10</sup> that Process (1a) could quantitatively explain the dissociation of  $I_2(X)$  in  $O_2^*$ . A number of recent observations cast considerable doubt on this conclusion. Houston and coworkers<sup>11</sup> found by direct laser pumping of  $O_2(^1\Sigma)$  in the presence of  $I_2$  that the total  $^1\Sigma$  removal rate coefficient ( $2 \times 10^{-11}$  cm<sup>3</sup>/molecule-sec) was 10 times smaller than the value of  $k_{1a}$  needed by Derwent and Thrush<sup>10</sup> to model their results. Muller et al.<sup>12</sup> estimated  $k_{1a}/k_1 < 0.2$ , although they determined that  $k_1 = 7 \times 10^{-11}$  cm<sup>3</sup>/molecule-sec. A lower value for  $k_{1a}$  was consistent with the failure of laser modeling codes to predict the rate of  $I_2$  dissociation in the continuous-wave transfer laser devices.<sup>13</sup> The principal obstacle to the modeling was the presence of  $H_2O$ , which served as a rapid quencher of  $O_2(^1\Sigma)$ . Experiments in our laboratory supported the claim that  $O_2(^1\Sigma)$  could be removed by  $H_2O$  without totally suppressing  $I_2$  dissociation,<sup>14</sup> and led to the conclusion that, although  $O_2(^1\Sigma)$  may be necessary, it is not sufficient to explain the rate of  $I_2$  dissociation in  $O_2^*$ .

The study described in this report is a major extension of the work reported in Ref. 14. The dissociation of  $I_2$  into atoms has been measured as a function of  $[O_2(^1\Delta)]$ ,  $[O_2(^3\Sigma)]$ ,  $[I_2]_0$ ,  $[H_2O]$ ,  $[Ar]$ , and qualitatively as a function of  $[I]_0$ . The dissociation curves for  $I_2$  versus time exhibit a rather unusual behavior, which are summarized as follows:

- <sup>8</sup>R. G. Derwent, D. R. Kearns, and B. A. Thrush, Chem. Phys. Lett. 6, 115 (1970).
- <sup>9</sup>R. G. Derwent and B. A. Thrush, Chem. Phys. Lett. 9, 591 (1971).
- <sup>10</sup>R. G. Derwent and B. A. Thrush, J. Chem. Soc. Faraday II, 68, 720 (1972).
- <sup>11</sup>R. G. Aviles, D. F. Muller, and P. L. Houston, Appl. Phys. Lett. 37, 358 (1980).
- <sup>12</sup>D. F. Muller, R. H. Young, P. L. Houston, and J. R. Wiesenfeld, Appl. Phys. Lett. 38, 404 (1981).
- <sup>13</sup>R. F. Shea, private communication.
- <sup>14</sup>R. F. Heidner III, C. E. Gardner, T. M. El-Sayed, and G. I. Segal, Chem. Phys. Lett. 81, 142 (1981)

1. "Initiator" effects [ $O(^3P)$  atoms,  $O_2(^1\Sigma)$ ...] are extremely important.
2. The curves often exhibit a substantial induction time.
3. Small amounts of  $H_2O$  strongly affect the dissociation rate, and large  $H_2O$  densities have a proportionately smaller effect.
4. The inverse half-life for dissociation,  $(t_{1/2})^{-1}$ , is proportional to  $[^1\Delta]^2 [^3\Sigma]^{-1} [I_2]_0^{-0.7} [Ar]^0$  over the concentration ranges studied.

These data indicate that  $I^*$  is strongly implicated in the dissociation process. We propose that the dissociation mechanism involves chain branching with  $I^*$  as the chain carrier. In the following sections we review the computer-controlled flow tube apparatus used to obtain these data. An analytic model is developed to simulate the experimental curves, rapidly test the model's sensitivity to various reactions and rate coefficients, and predict the scaling of the dissociation kinetics into laser-like concentration regimes. A limited number of numerical modeling calculations then is presented for all the measurable system species concentrations. The time behavior of  $O_2(^1\Delta)$  is particularly crucial. Some sets of modeling parameters can correctly reproduce the  $I_2$  dissociation curves; however, they predict an unrealistically large removal of  $O_2(^1\Delta)$  molecules for each  $I_2$  dissociated.



## II. EXPERIMENTAL APPARATUS

The computer-controlled flow tube apparatus (Fig. 2) has been extensively described in earlier publications.<sup>4,14</sup> Electronically excited oxygen is created by conventional microwave discharge techniques. The  $O(^3P)$  atoms created in the discharge are recombined on a heated HgO mirror deposited downstream of the discharge cavity by co-discharging Hg +  $O_2$  prior to a set of experiments. The earlier apparatus was modified to permit a variable fraction of the  $O_2$  to be passed through the discharge; the remainder is added downstream of the discharge, but well upstream of the  $I_2$  addition port.

The principal injected gases in this study were  $I_2(+Ar)$  and  $H_2O(+Ar)$ . We continue to use the method of flow replacement, whereby a pure Ar stream is gradually replaced with an  $I_2 + Ar$  (or  $H_2O + Ar$ ) mixture to vary minority constituent densities without changing total molar flow or total pressure. Elevated temperature saturators were employed to produce the appropriate mole fractions of  $I_2$  and  $H_2O$  in Ar. The saturation efficiency was tested under flowing conditions by visible absorption spectroscopy ( $I_2$ ) and by sampled gas analysis ( $H_2O$ ).

The flow tube is constructed from 38.5 mm i.d. Pyrex internally coated with halocarbon wax. The usable length of the tube is 60 cm. Two types of  $I_2$  injectors were used. The first injected  $I_2$  axially through a six-prong spoke injector, in which each prong had four holes  $\sim 0.5$  mm in diameter. The second "ring" injector used eight holes  $\sim 1$  mm in diameter, drilled radially in the flow tube walls. This latter technique was generally used.

As in our previous studies,<sup>4,14</sup> the optical emission features  $O_2(^1\Delta + ^3\Sigma)$  ( $\lambda = 1.27 \mu m$ ),  $I(^2P_{1/2} + ^2P_{3/2})$  ( $\lambda = 1.315 \mu m$ ),  $O_2(^1\Sigma + ^3\Sigma)$  ( $\lambda = 0.762 \mu m$ ), and  $I_2(B^3\Pi_u + X^1\Sigma_g^+)$  ( $\lambda_{max} = 0.580 \mu m$ ) were monitored by two spectrometer systems mounted on a movable platform. This platform is moved to discrete positions on the flow tube by a computer-controlled stepping motor. At each flow tube position, the emission intensity monitored by each spectrometer system is sampled by the computer. During this work, it was found necessary

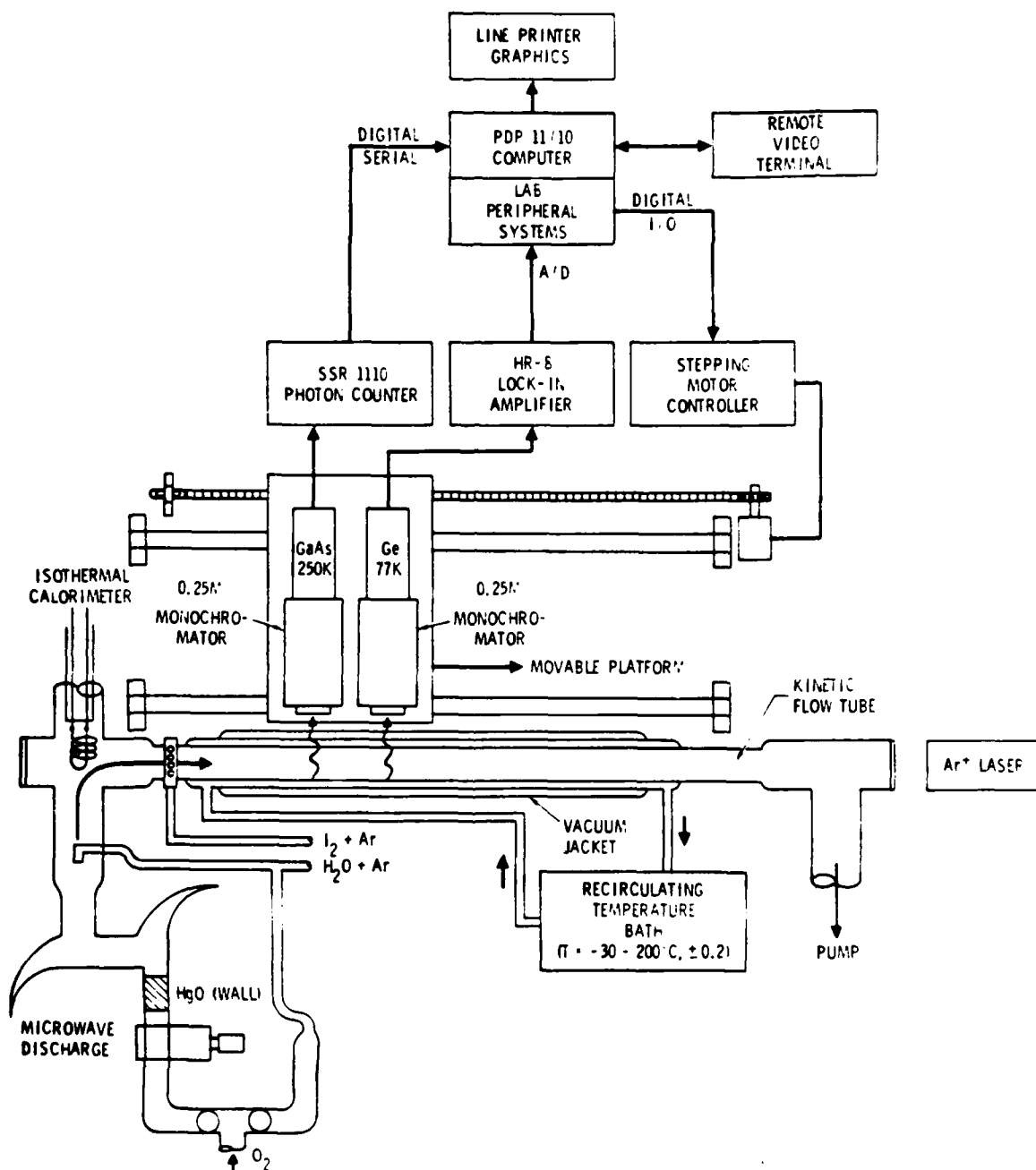


**Fig. 2. Schematic Diagram of the Computer-Controlled Kinetic Flow Tube Apparatus.**

to monitor a near-infrared emission system<sup>15</sup> (Fig. 3) that has been identified as  $I_2(A \rightarrow X)$  emission from  $v' = 0$  and 1.<sup>16</sup> Under some conditions, a difference spectrum must be computed to accurately determine the  $O_2(^1\Delta)$  emission intensity at 1.27  $\mu m$ . Our empirical procedure involves subtracting the emission intensity at 1.24  $\mu m$  (pure  $A \rightarrow X$ ) from that at 1.27  $\mu m$  [ $O_2(^1\Delta + ^3\Sigma)$  plus  $I_2(A \rightarrow X)$ ]. Five species are monitored by optical emission spectroscopy, requiring three scans of the flow tube under fixed experimental conditions. The procedure for converting optical emission signals to absolute densities is described in Ref. 4. Absolute densities are determined for  $[^1\Delta]$ ,  $[^1\Sigma]$ ,  $[I^*]$ , and computed by mass balance for  $[I_2]$ . Relative measurements only are reported for  $[I_2(A)]$  and  $[I_2(B)]$ . Mixing efficiency is an issue in these experiments for several reasons. We have suggested that  $I^*$  is implicated in the  $I_2$  dissociation process. Thus, the analysis implicitly assumes that  $I_2$  (and  $I^*$ ) are homogeneously mixed during the dissociation process. In addition, if mixing is slow, we are forced to work at relatively long dissociation times, where  $I$  atom recombination complicates the analysis. Figure 4 shows that  $I_2$  mixing into the  $O_2$  flow can be optimized for a specific flow tube geometry by injecting Ar diluent in with the  $I_2$ . Using the radial ring injector, the mixing was studied by means of  $I_2(B \rightarrow X)$  laser-induced fluorescence (LIF) pumped at 514.5 nm by a repetitively pulsed  $Ar^+$  laser (TRW model 71B; 40  $\mu J$ /pulse) and monitored by the photon counting system. In Fig. 4, it can be seen that a relatively small amount of added diluent causes the centerline mixing to approach a step function. All data reported in this flow tube study are sampled every 1.25 cm at flow velocities ( $< 550$  cm/sec) that are within a factor of 2 of that used in Fig. 4. With a modulated continuous wave  $Ar^+$  laser, it is possible to get  $I_2$  dissociation curves directly, even in the presence of background  $I_2(B \rightarrow X)$  emission.

<sup>15</sup>R. F. Heidner III, Spectroscopic Properties of the  $O_2^* - I_2$  Flame, TR-0082(2610)-1, The Aerospace Corporation, El Segundo, California (to be published).

<sup>16</sup>S. J. Davis and P. D. Whitefield, to be published.

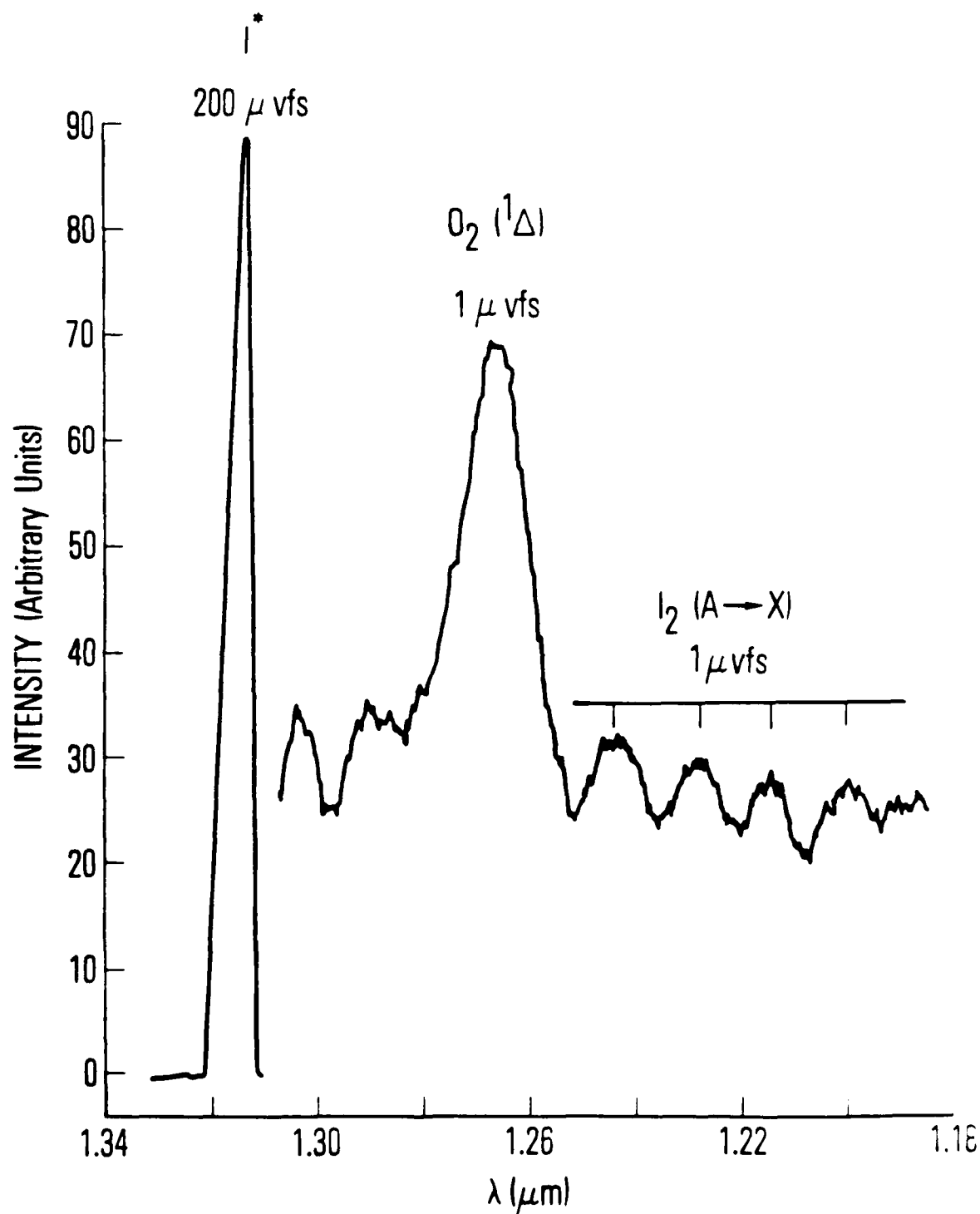


Fig. 3. Low Resolution Spectrum of the  $\text{I}_2(\text{A} \rightarrow \text{X})$  Transition Underlying the Spectrum of  $\text{O}_2({}^1\Delta + {}^3\Sigma)$  and  $\text{I}({}^2\text{P}_{1/2} + {}^4\text{P}_{3/2})$ .

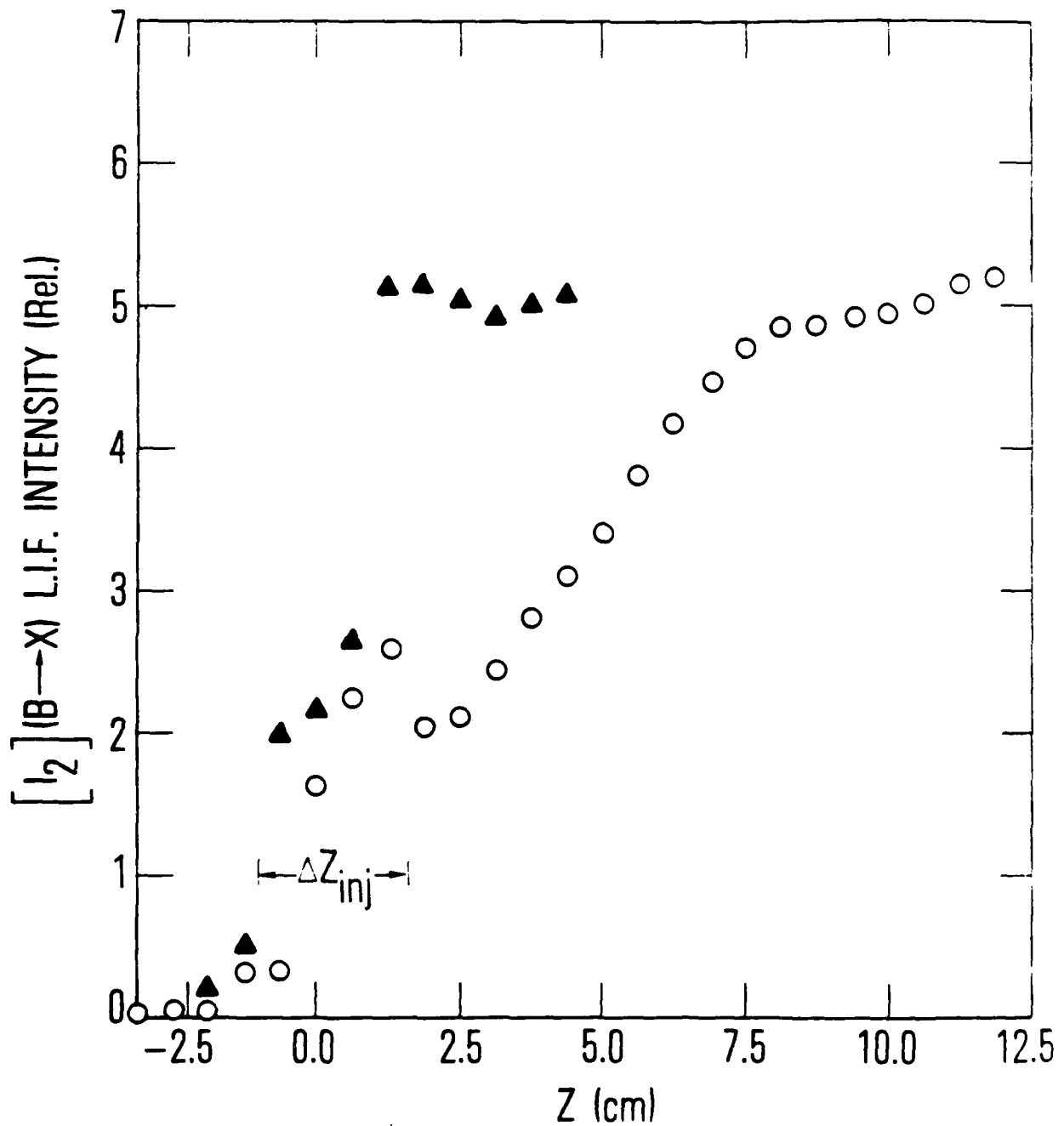
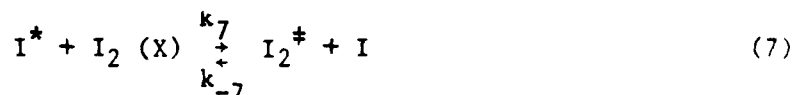


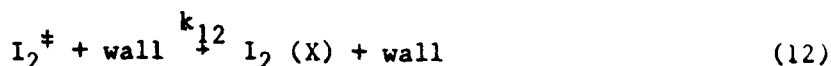
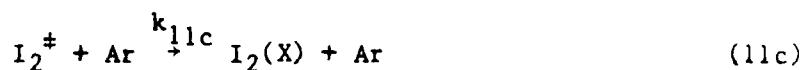
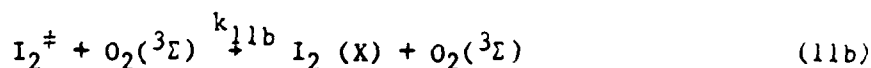
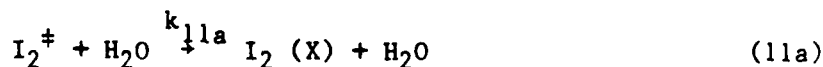
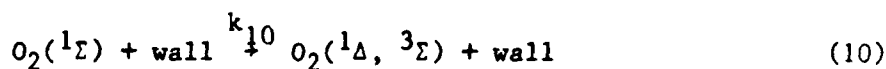
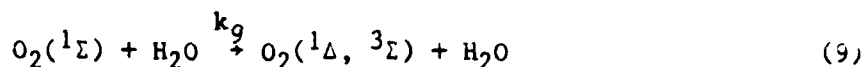
Fig. 4. Mixing Efficiency of  $I_2(+Ar)$  into  $O_2$  Using the Radial Injector (Fig. 2): O- $I_2$  + Ar Mixture from the Saturator;  $\Delta$  - Additional Pure Ar Injected with  $I_2$  + Ar Mix. Optical distortion occurs within  $\Delta Z_{inj}$ . Plug flow velocity = 250 cm/sec.

### III. ANALYTIC MODELING OF $I_2$ DISSOCIATION

Several processes are considered in addition to Processes (1) through (6). It was proposed that  $I^*$  participates directly in the  $I_2$  dissociation process. Although Process (3) satisfies that criterion qualitatively, we will consider two additional processes:

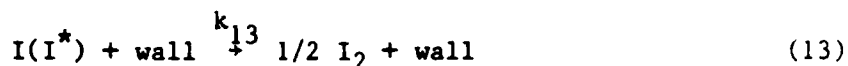


Removal rate coefficient data exist for  $I^* + I_2(X)$ . Nothing is presently known about Process (8). Quenching of  $O_2(^1\Sigma)$  and  $I_2^\ddagger$  must be considered to complete a simple analytic model:



Quenching of  $I_2^\ddagger$  by  $I_2(X)$  has been carefully considered and rejected as a major process, because it predicts the wrong dependence of the dissociation rate on  $[I_2]_0$ . A recombination term for I atoms must be included to represent

the experimental observation of residual  $I_2$  in the steady-state flow for certain initial values of  $O_2(^1\Delta)$  and  $I_2$ . Under low pressure flow tube conditions, this process must certainly be wall recombination:



Because one of the primary goals of the analytic modeling is the sensitivity analysis for various processes, Process (13) will be ignored initially to obtain a relatively simple expression. An exact solution is still possible with Process (13) included, and this solution will be discussed. The contribution from the  $O_2(^1\Sigma)$  model and the sequential excitation model will be formally separated. The rate processes considered in these models are summarized in Table 1.

#### A. STEADY-STATE $O_2(^1\Sigma) + I_2$ MODEL

Using definitions for  $[I^*]$ ,  $R_\Sigma(\text{sec}^{-1})$ , and  $[O_2(^1\Sigma)]_{ss}$  developed in Appendix A, the removal of  $I_2$  by  $O_2(^1\Sigma)$  can be written

$$\begin{aligned} -\frac{d[I_2]}{dt} &= k_{1a} [^1\Sigma]_{ss} [I_2] \\ &= a_\Sigma [I_2] - b_\Sigma [I_2]^2 \end{aligned} \quad (14)$$

$$\text{where } a_\Sigma = \left[ \frac{k_3 k_{1a}}{R_\Sigma} \right] [^1\Delta]^2 \left\{ \frac{k_2}{k_3} + \frac{K_{EQ}}{[^3\Sigma]} \left( \frac{2}{(1+X)} [I_2]_0 + [I]_0 \right) \right\}$$

$$b_\Sigma = \left[ \frac{k_3 k_{1a}}{R_\Sigma} \right] [^1\Delta]^2 \left( \frac{2K_{EQ}}{(1+X) [^3\Sigma]} \right)$$

$$X = K_{EQ} [^1\Delta] / [^3\Sigma]$$

Table 1. Kinetic Model of  $I_2$  Dissociation by  $O_2^*$  ( $T = 295\text{ K}$ )

Process	Rate Coefficient (cm <sup>3</sup> /molecule-sec)	Reference
$O_2(^1\Sigma) + I_2(X) \xrightarrow{k_{1a}} O_2(^3\Sigma) + 2I$	$4 \times 10^{-12}$	(a) 11
	$< 1.6 \times 10^{-11}$	12
$k_1$ All Products	$(2.06 \pm 0.28) \times 10^{-11}$	(b) 11
	$7 \times 10^{-11}$	12
$O_2(^1\Delta) + O_2(^1\Delta) \xrightarrow{k_2} O_2(^1\Sigma) + O_2(^3\Sigma)$	$(2.0 \pm 0.5) \times 10^{-17}$	2
$O_2(^1\Delta) + I^* \xrightarrow{k_3} O_2(^1\Sigma) + I$	$(1.1 \pm 0.3) \times 10^{-13}$	4
$O_2(^1\Delta) + I \xrightarrow[k_{-4}]{k_4} O_2(^3\Sigma) + I^*$	$k_{-4} \approx (2.6 \pm 0.6) \times 10^{-11}$	25, 26
	$[k_4 \approx (7.6 \pm 2.5) \times 10^{-11}]$	(c)
$O_2(^1\Delta) + I_2(X) \xrightarrow[k_{-5}]{k_5} O_2(^3\Sigma) + I_2^*$	Table 5	This Work
$O_2(^1\Delta) + I_2^* \xrightarrow{k_6} O_2(^3\Sigma) + 2I$	Table 5	This Work
$I^* + I_2(X) \xrightarrow[k_{-7}]{k_7} I + I_2^*$	$< (1.5 \pm 0.5) \times 10^{-11}$	(d) 27, 28
$I_2^* + I^* \xrightarrow{k_8} 3I$	Table 5	This Work

25. I. Deaklin and D. Muecke, *J. C. S. Faraday II*, **68**, 41 (1972).  
 26. H. Burda and R. S. MacFarlane, *J. Chem. Phys.*, **66**, 1850 (1976).  
 27. A. I. Grigoryev and V. I. Houston, *J. Chem. Phys.*, **68**, 3366 (1978).  
 28. H. Hofmann and G. V. Leone, *J. Chem. Phys.*, **69**, 641 (1978).



Table 1. Kinetic Model of  $I_2$  Dissociation by  $O_2^*$  (T = 295 K) (Continued)

Process	Rate Coefficient (cm <sup>3</sup> /molecule-sec)	Reference
$O_2(^1\Sigma) + H_2O \xrightarrow{k_9} O_2(^1\Delta, ^3\Sigma) + H_2O$	$(5.5 \pm 1) \times 10^{-12}$	2,11
$O_2(^1\Sigma) + wall \xrightarrow{k_{10}} O_2(^1\Delta, ^3\Sigma) + wall$	$20 \text{ s}^{-1} (\gamma = 3 \times 10^{-3})$	(e) 4
$I_2^* + H_2O \xrightarrow{k_{11a}} I_2(X) + H_2O$	Table 5	This Work
$I_2^* + O_2 \xrightarrow{k_{11b}} I_2(X) + O_2$	Table 5	This Work
$I_2^* + Ar \xrightarrow{k_{11c}} I_2(X) + Ar$	Table 5	This Work
$I_2^* + wall \xrightarrow{k_{12}} I_2(X)$	Table 5	This Work
$I(I^*) + wall \xrightarrow{k_{13}} 1/2 I_2(X) + wall$	Table 5	This Work

<sup>a</sup>The value for  $k_{1a}$  was calculated from the  $k_{1a}/k_1$  result from Ref. 12.

<sup>b</sup>The authors of Ref. 12 imply that  $k_1$  determined in Ref. 11 is to be preferred.

<sup>c</sup>The value of  $k_4$  is calculated from  $k_{-4}$  by statistical mechanics ( $K_{eq} = 2.9$  at T = 295 K).

<sup>d</sup>The reported value is the  $I^*$  removal rate coefficient.

<sup>e</sup> $\gamma = (2R k_{10})/c$ , where  $c$  is the oxygen mean velocity and  $R$  is the tube radius.

This formalism and that for sequential excitation, which follows, assume that the  $[^1\Delta]$  and  $[^3\Sigma]$  are constant during the dissociation. Both analyses allow for the presence of I atoms at  $t = 0$ .

#### B. SEQUENTIAL MODEL WITH $I_2^+$ IN STEADY STATE

The analysis of the sequential model depends upon the relative importance of Processes (7) and (8). The general expression can be derived by defining the quenching term for  $I_2^+$ ,  $R_{I_2^+}$ , and writing down a steady-state expression for  $[I_2^+]$  (Appendix A). At this juncture, we are only hypothesizing that  $I_2^+$  is in steady state:

$$\begin{aligned} - \frac{d[I_2]}{dt} &= (k_5 [^1\Delta] + k_7 [I^*]) [I_2] \\ &- ([ (k_{-5} + k_{11b}) [^3\Sigma] + k_{-7} [I] + k_{11a} [H_2O] + k_{11c} [Ar] \\ &\quad + k_{12} ]) [I_2^+]_{ss} \\ &= a_{SQ} [I_2] - b_{SQ} [I_2]^2 \end{aligned} \tag{15}$$

where

$$a_{SQ} = \frac{k_5 k_6}{R_{I_2^+}} [^1\Delta]^2 \left\{ 1 + \left( \frac{k_8}{k_6} + \frac{k_7}{k_5} \right) \frac{k_{EQ}}{[^3\Sigma]} \left[ \frac{2}{(1+X)} [I_2]_0 + [I]_0 \right] \right\}$$

and

$$b_{SQ} = \frac{k_5 k_6}{R_{I_2^+}} [^1\Delta]^2 \left( \frac{k_8}{k_6} + \frac{k_7}{k_5} \right) \frac{2 k_{EQ}}{[^3\Sigma] (1+X)}$$

A term in  $[I^*]^2$  has been neglected in the derivation of Eq. (15). This assumption is examined in Section IV.

### C. GLOBAL ANALYTIC EQUATION

Equations (14) and (15) can be combined to give a single differential equation

$$-\frac{d[I_2]}{dt} = (a_L + a_{SQ}) [I_2] - (b_L + b_{SQ}) [I_2]^2 \quad (16)$$

that can be integrated into the following expression:

$$\frac{(a - b[I_2])/[I_2]}{(a - b[I_2]_0)/[I_2]_0} = \exp(at) \quad (17)$$

or

$$[I_2] = \frac{c}{1 + \exp(at) (c/[I_2]_0 - 1)} \quad (18)$$

where  $a = a_L + a_{SQ}$ ,  $b = b_L + b_{SQ}$ , and  $c = a/b$ . Because the  $I_2$  decays are not exponential, it is useful to define a dissociation half-life,  $t_{1/2}$ :

$$\begin{aligned} t_{1/2} &= a^{-1} \ln \left( \frac{2c - [I_2]_0}{c - [I_2]_0} \right) \\ &= a^{-1} \ln \left( \frac{[I_2]_0}{c'} + 2 \right) \end{aligned} \quad (19)$$

$$\text{where } c' = \frac{(1 + X)}{2} \left( [I]_0 + \frac{\rho}{K_{EQ}} [^3I] \right) \text{ and } \rho = \frac{K_L(1) + K_{SQ}(1)}{K_L(2) + K_{SQ}(2)}$$

The parameters in Eqs. (14) through (19) have been categorized in Table 2, so that they can be useful for sensitivity analysis. The strongest variation in Eq. (19) is in the term  $a$ , which consists of two subterms: ignoring  $R_{\Sigma}$  and  $R_{I\ddagger}$  for the moment, the first scales as  $[^1\Delta]^2 [I_2]_0 / [^3\Sigma]$  (assuming  $[I]_0 \ll [I_2]_0$  and  $X \ll 1$ ) and the second as  $[^1\Delta]^2$ . As indicated in Table 2, the  $O_2(^1\Sigma)$  mechanism ( $a_{\Sigma}$ ) and the sequential excitation mechanism ( $a_{SQ}$ ) each contributes to these two subterms. Direct measurements of  $k_{1a}$  ( $\sim 0.2 k_1$ ),  $k_2$ ,  $k_3$ ,  $k_9$ , and  $k_{10}$  (Table 1) permit a quantitative evaluation of  $a_{\Sigma}$ . In Section IV, we show that the magnitude of  $a_{\Sigma}$  cannot explain the observed dissociation rates. Although this conclusion was reached in our preliminary work,<sup>14</sup> the present study will show a role for the  $O_2(^1\Sigma)$  mechanism as a dissociation initiator.

Table 2. Analytic Dissociation Model Parameters<sup>a</sup>

$a_i$ (sec <sup>-1</sup> )	Equivalent Coefficients			Definitions
	I <sub>Σ</sub> Model $[K_T(I)]^b$	Sequential Model $[K_{S0}(I)]^c$	Concentration Dependence <sup>d,e</sup> ( $X_1$ )	
$a_1$	$\frac{k_{1a}k_2}{R_\Sigma}$	$\frac{k_5k_6}{R_{1,2}^\ddagger}$	$[I_A]^2$	$a_1 = [K_T(I) + K_{S0}(I)] X_1$
$a_2$	$\frac{k_{1a}k_3}{R_\Sigma}$	$\frac{k_5k_8 + k_6k_7}{R_{1,2}^\ddagger}$	$K_{F0} \frac{[I_A]^2}{[I_2]^\ddagger} (1 + X) [I_2] + [I_1]_0$	$a_2 = [K_T(I) + K_{S0}(I)] X_1$
$b_1$	$\frac{k_{1a}k_3}{R_\Sigma}$	$\frac{k_5k_8 + k_6k_7}{R_{1,2}^\ddagger}$	$\frac{2 K_{F0}}{(1 + X)} \frac{[I_A]^2}{[I_2]^\ddagger}$	$b_1 = [K_T(I) + K_{S0}(I)] X_1$
$b$				$b = b_1 (= b_T + b_{S0})$

<sup>a</sup>  $b_1$  (molecule-sec)

$$a_1 I_2 / 2 = a^{-1} \ln ((2(a/b) - [I_2]_0) / (a/b) - [I_2]_0) \quad [\text{Eq. (19)}]$$

$$b R_\Sigma = k_9 [H_2O] + k_1 [I_2]_{ss} + k_{10}$$

$$R_{T2}^\ddagger = k_6 [I_A] + k_{-5} [I] + k_8 [I] + k_7 [I] + k_{11a} [H_2O] + k_{11b} [I] + k_{Ar} [Ar] + k_{12}$$

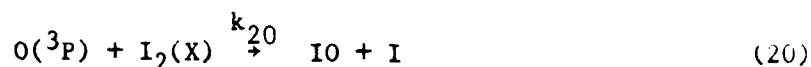
<sup>d</sup> If  $O_2(I_\Sigma)$  and  $I_2^\ddagger$  removal are not dominated by radiative or wall losses, the terms  $R_T$  and  $P_{1,2}^\ddagger$  have implicit concentration dependences.

$$X = K_{F0} [I_A] / [I_\Sigma]; \quad K_{F0} = k_6 / k_{-4}$$

#### IV. RESULTS AND DISCUSSION

##### A. INITIATION EFFECTS AND INDUCTION TIMES

In Fig. 5, the effect of dissociation initiators is clearly evident. The experimental growth of  $I^*$  signal ( $\lambda = 1.315 \mu\text{m}$ ) is shown as a function of time. The decay of  $I_2(X)$  is computed from these data using Eq. (A3) from Appendix A. The two experiments shown differ in only one respect: Curve A has 10% of the  $O_2$  and Curve B has 100% of the  $O_2$  passed through the microwave discharge. Under the latter conditions, some of the  $O(^3P)$  atoms from the discharge are swept over the heated  $HgO$  surface without being recombined. Subsequently, the fast reaction<sup>17</sup>



introduces  $I$  atoms into the system. Regardless of the initial state of the  $I$  atoms formed in Process (20),  $I^*$  is rapidly produced by Process (4).

The interesting portion of the traces in Fig. 5 occurs after the  $O(^3P)$  atoms are titrated by  $I_2$  ( $t \gtrsim 15 \text{ msec}$ ). Curve A shows a long induction time for the dissociation process; Curve B reaches its asymptotic level of dissociation at approximately 160 msec. Identical kinetic behavior is observed if the dissociation is initiated by  $O_2(^1\Sigma)$  that is formed by Process (2).

Small amounts of added  $H_2O$  have a rather large effect on the  $I_2$  dissociation rate. The  $[^1\Sigma]_0$  formed by Process (2) can significantly initiate the dissociation by means of Process (1a) if  $H_2O$  has not made  $[^1\Sigma]_0$  insignificant with respect to  $[I_2]_0$  [see Eq. (A4)]. The effect of larger amounts of  $H_2O$  on the system will be treated later in this section.

<sup>17</sup>D. St. A. G. Radlein, J. C. Whitehead, and R. Grice, *Mol. Phys.* 29, 1813 (1975).

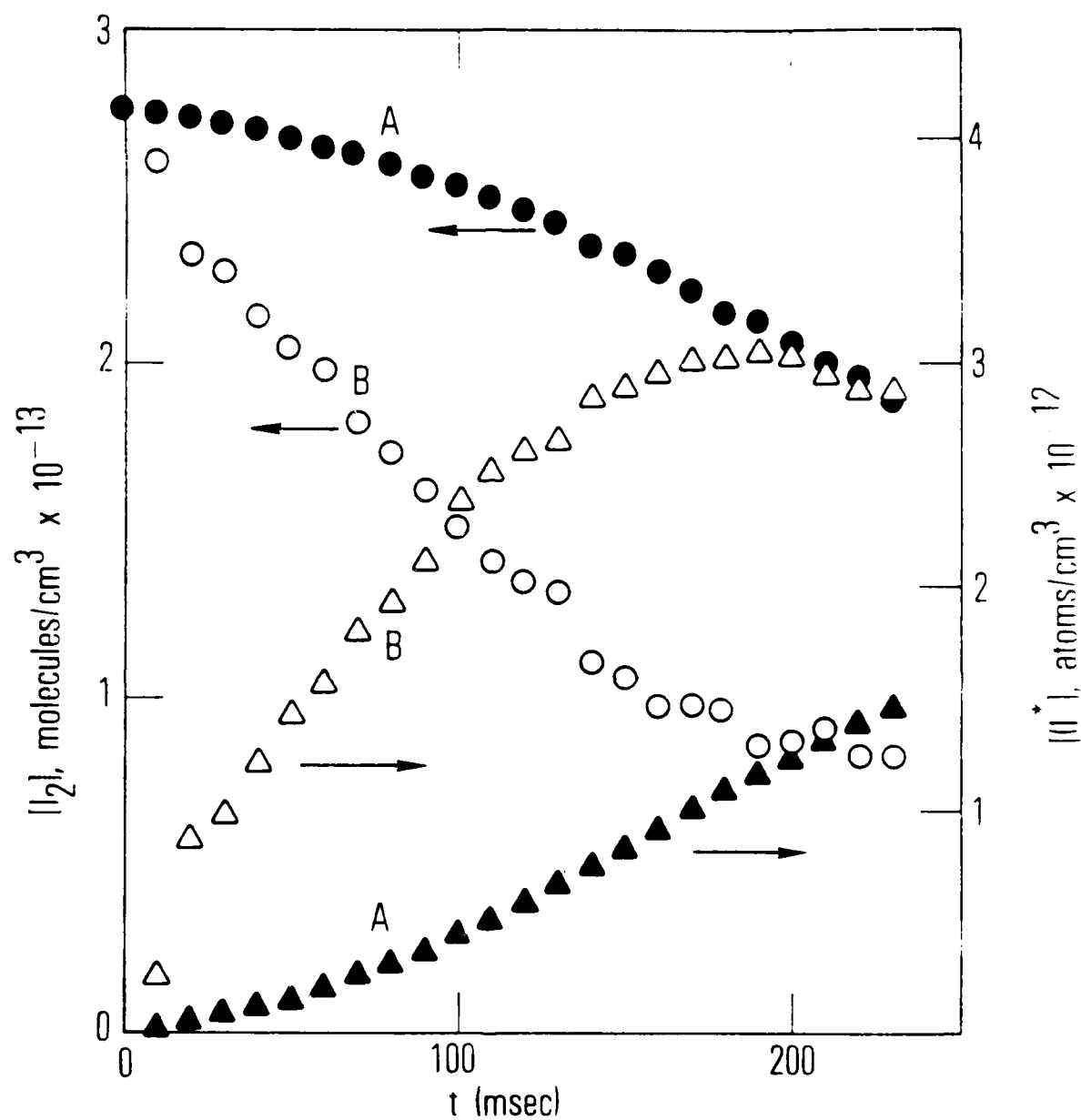


Fig. 5. Effect of  $O(^3P)$  on Dissociation Initiation.

● =  $I_2$ ; △ =  $I^*$ : 10% of  $O_2$  discharged (A);  
 ○ =  $I_2$ ; △ =  $I^*$ : 100% of  $O_2$  discharged (B);  
 $[^1\Delta] = 1.6 \times 10^{15}/\text{cm}^3$ ;  $[^3\Sigma] = 7.1 \times 10^{16}/\text{cm}^3$ ;  
 $[H_2O] = 6.4 \times 10^{14}/\text{cm}^3$ ;  $[Ar] = 1.9 \times 10^{16}/\text{cm}^3$ ;  
 $[O(^3P)]_0 = 4 \times 10^{12}/\text{cm}^3$  (B).

By ensuring that all I atom sources [ $O(^3P)$ ,  $O_2(^1\Sigma)$ , . . .] are rigorously suppressed at  $t = 0$ , one can study the intrinsic induction time for  $I_2$  dissociation. The  $O_2(^1\Sigma)$  model alone cannot accurately predict  $I_2$  dissociation profiles under these conditions. Table 2 (which must be supplemented by Appendix B if the wall recombination rate  $k_{13}$  cannot be ignored) shows that the general model reduces to the  $O_2(^1\Sigma)$  model if both  $k_5$  and  $k_6$  are zero.

For conditions where  $[H_2O] \gg [I_2]_0$  and  $[I]_0 = 0$ , we can write the dissociation half-life from Eq. (19) as follows:

$$t_{1/2} = a^{-1} \ln \left( \frac{[I_2]_0}{c'} + 2 \right) \quad (21)$$

$$\text{where } c' = \left( \frac{k_2}{k_3} \right) \frac{(1+X) [^3\Sigma]}{2 K_{EQ}} \text{ and } a = \left( \frac{k_{1a}}{R_\Sigma} \right) [^1\Delta]^2 \left[ k_2 + \frac{2 K_{EQ} [I_2]_0}{(1+X) [^3\Sigma]} k_3 \right]$$

All the rate parameters in Eq. (21) are known from independent experiments. Figure 6 gives an experimental data set satisfying all the conditions stated above. Several calculations are shown using rate coefficients taken from Table 1 to evaluate Eq. (21), or more precisely, Eq. (18). In one calculation the value of  $k_{1a}$  ( $2 \times 10^{-10}$  cm<sup>3</sup>/molecule-sec) originally recommended by Derwent and Thrush is used. In two others, direct measurements of  $k_1$  and  $k_{1a}$  made by Houston and coworkers are used. None of these calculations can accurately represent the rate of  $I_2$  dissociation over the full range of experimental conditions presented in Table 3 (particularly at large  $[H_2O]/[I_2]$  values). Nevertheless, we have made numerical calculations for  $I_2$  dissociation under our experimental conditions using a gas kinetic rate coefficient ( $3 \times 10^{-10}$  cm<sup>3</sup>/molecule-sec) for  $k_{1a}$  and standard rate coefficients (Table 1) for other important processes. The agreement with experiment is moderately good (Table 4), but based on the direct measurements of Houston and coworkers,<sup>11,12</sup> such agreement must be fortuitous.

One can attempt to initiate the dissociation more strongly in the model by including the term  $K_{SQ}(1)$  (Table 2) that represents a sequential process



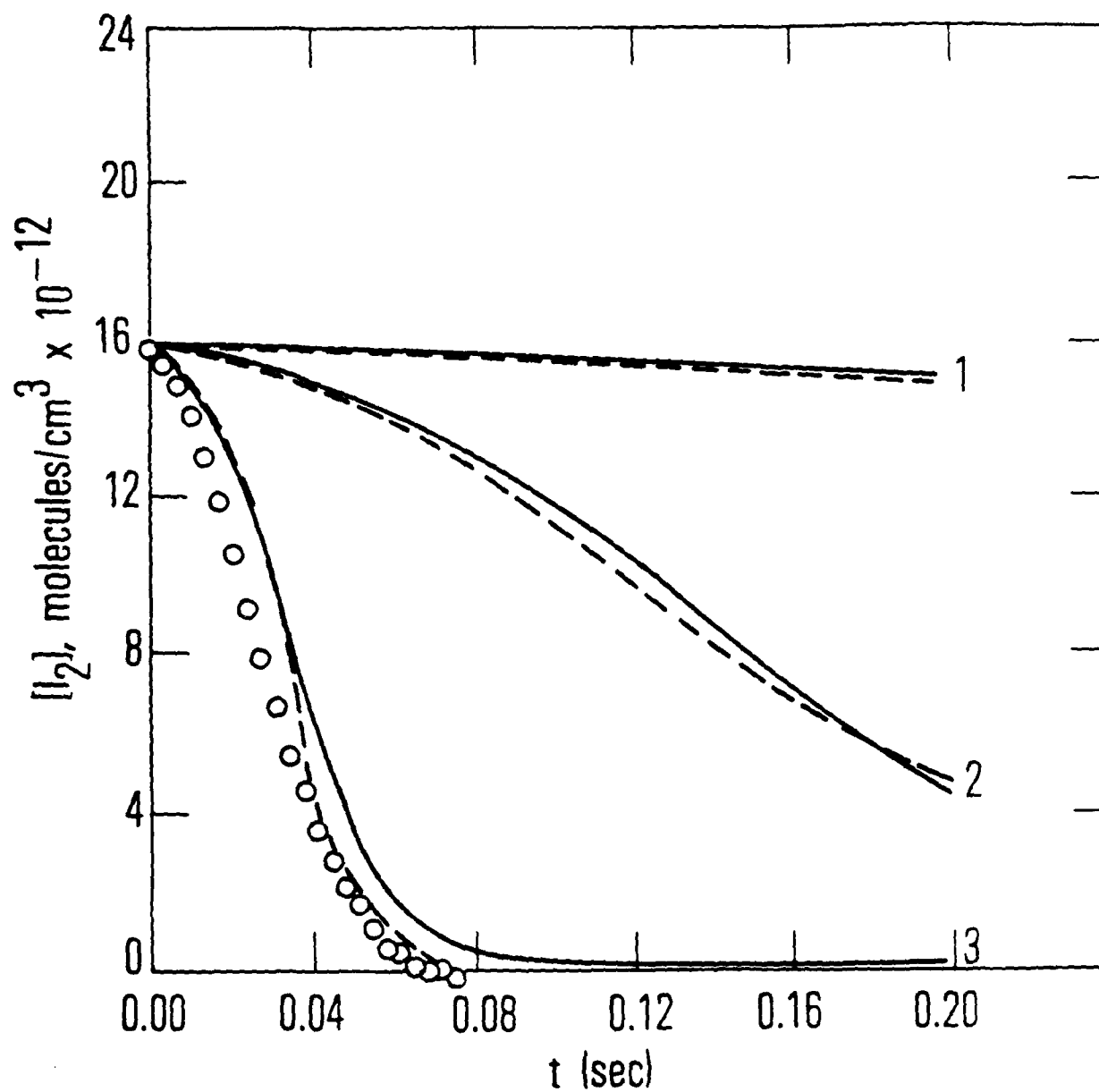


Fig. 6.  $I_2$  Dissociation by Means of the  $^1\Sigma + I_2$  Mechanism  
 Curve 1:  $k_1 = 2 \times 10^{-11}$ ;  $k_{1a}/k_1 = 0.2$  (Refs. 11 and 12)  
 Curve 2:  $k_1 = 2 \times 10^{-11}$ ;  $k_{1a}/k_1 = 1$  (Refs. 11 and 12)  
 Curve 3:  $k_1 = 2 \times 10^{-10}$ ;  $k_{1a}/k_1 = 1$  (Refs. 10)  
 Data: Run A3, Table 3. Analytic fits (----); numerical fits (---).

Table 3. Experimental Conditions and I<sub>2</sub> Dissociation Half-Lives

Run	t <sub>1/2</sub> , sec	O <sub>2</sub> ( <sup>3</sup> Σ), molecules/cm <sup>3</sup>	O <sub>2</sub> ( <sup>1</sup> Δ), molecules/cm <sup>3</sup>	O <sub>2</sub> ( <sup>1</sup> Σ), molecules/cm <sup>3</sup>	I <sub>2</sub> , molecules/cm <sup>3</sup>	H <sub>2</sub> O, molecules/cm <sup>3</sup>	Ar, molecules/cm <sup>3</sup>
O <sub>2</sub> ( <sup>1</sup> Δ) Variation							
A1	0.020	2.0 × 10 <sup>16</sup>	2.5 × 10 <sup>15</sup>	1.0 × 10 <sup>11</sup>	1.6 × 10 <sup>13</sup>	2.2 × 10 <sup>14</sup>	6.9 × 10 <sup>16</sup>
A2	0.025	2.0 × 10 <sup>16</sup>	2.3 × 10 <sup>13</sup>	8.4 × 10 <sup>10</sup>	1.6 × 10 <sup>13</sup>	2.2 × 10 <sup>14</sup>	6.9 × 10 <sup>16</sup>
A3	0.034	2.0 × 10 <sup>16</sup>	1.9 × 10 <sup>15</sup>	6.0 × 10 <sup>10</sup>	1.6 × 10 <sup>13</sup>	2.2 × 10 <sup>14</sup>	6.9 × 10 <sup>16</sup>
A4	0.051	2.0 × 10 <sup>16</sup>	1.6 × 10 <sup>15</sup>	4.0 × 10 <sup>10</sup>	1.6 × 10 <sup>13</sup>	2.2 × 10 <sup>14</sup>	6.9 × 10 <sup>16</sup>
A5	0.082	2.0 × 10 <sup>16</sup>	1.3 × 10 <sup>15</sup>	2.7 × 10 <sup>10</sup>	1.6 × 10 <sup>13</sup>	2.2 × 10 <sup>14</sup>	6.9 × 10 <sup>16</sup>
A6	0.156	2.0 × 10 <sup>16</sup>	9.5 × 10 <sup>14</sup>	1.5 × 10 <sup>10</sup>	1.6 × 10 <sup>13</sup>	2.2 × 10 <sup>14</sup>	6.9 × 10 <sup>16</sup>
O <sub>2</sub> ( <sup>3</sup> Σ) Variation							
R1	0.047	1.4 × 10 <sup>16</sup>	1.6 × 10 <sup>15</sup>	1.4 × 10 <sup>10</sup>	2.9 × 10 <sup>13</sup>	6.6 × 10 <sup>14</sup>	7.7 × 10 <sup>16</sup>
R2	0.068	2.1 × 10 <sup>16</sup>	1.6 × 10 <sup>15</sup>	1.4 × 10 <sup>10</sup>	2.9 × 10 <sup>13</sup>	6.6 × 10 <sup>14</sup>	6.9 × 10 <sup>16</sup>
R3	0.094	2.9 × 10 <sup>16</sup>	1.6 × 10 <sup>15</sup>	1.4 × 10 <sup>10</sup>	2.9 × 10 <sup>13</sup>	6.6 × 10 <sup>14</sup>	6.1 × 10 <sup>16</sup>
R4	0.120	3.7 × 10 <sup>16</sup>	1.6 × 10 <sup>15</sup>	1.4 × 10 <sup>10</sup>	2.9 × 10 <sup>13</sup>	6.6 × 10 <sup>14</sup>	5.3 × 10 <sup>16</sup>
R5	0.165	5.2 × 10 <sup>16</sup>	1.6 × 10 <sup>15</sup>	1.4 × 10 <sup>10</sup>	2.9 × 10 <sup>13</sup>	6.6 × 10 <sup>14</sup>	3.9 × 10 <sup>16</sup>
R6	0.25	7.1 × 10 <sup>16</sup>	1.6 × 10 <sup>15</sup>	1.4 × 10 <sup>10</sup>	2.9 × 10 <sup>13</sup>	6.6 × 10 <sup>14</sup>	1.9 × 10 <sup>16</sup>
I <sub>2</sub> Variation							
C1	0.026	1.6 × 10 <sup>16</sup>	2.1 × 10 <sup>15</sup>	9.0 × 10 <sup>10</sup>	8.3 × 10 <sup>12</sup>	1.7 × 10 <sup>14</sup>	4.6 × 10 <sup>16</sup>
C2	0.016	1.6 × 10 <sup>16</sup>	2.1 × 10 <sup>15</sup>	9.0 × 10 <sup>10</sup>	1.8 × 10 <sup>13</sup>	1.7 × 10 <sup>14</sup>	4.6 × 10 <sup>16</sup>
C3	0.012	1.6 × 10 <sup>16</sup>	2.1 × 10 <sup>15</sup>	9.0 × 10 <sup>10</sup>	2.6 × 10 <sup>13</sup>	1.7 × 10 <sup>14</sup>	4.6 × 10 <sup>16</sup>
C4	0.0085	1.6 × 10 <sup>16</sup>	2.1 × 10 <sup>15</sup>	9.0 × 10 <sup>10</sup>	3.3 × 10 <sup>13</sup>	1.7 × 10 <sup>14</sup>	4.6 × 10 <sup>16</sup>
C5	0.009	1.6 × 10 <sup>16</sup>	2.1 × 10 <sup>15</sup>	9.0 × 10 <sup>10</sup>	5.1 × 10 <sup>12</sup>	1.7 × 10 <sup>14</sup>	4.6 × 10 <sup>16</sup>

Table 3. Experimental Conditions and I<sub>2</sub> Dissociation Half-Lives (Continued)

Run	t <sub>1/2</sub> , sec	O <sub>2</sub> ( <sup>3</sup> Σ) molecules/cm <sup>3</sup>	O <sub>2</sub> ( <sup>1</sup> Δ) molecules/cm <sup>3</sup>	O <sub>2</sub> ( <sup>1</sup> Σ) molecules/cm <sup>3</sup>	I <sub>2</sub> molecules/cm <sup>3</sup>	H <sub>2</sub> O molecules/cm <sup>3</sup>	Ar molecules/cm <sup>3</sup>
H <sub>2</sub> O Variation							
D1	0.002	1.4 × 10 <sup>16</sup>	1.6 × 10 <sup>15</sup>	2.4 × 10 <sup>12</sup>	9.3 × 10 <sup>12</sup>	0	4.4 × 10 <sup>16</sup>
D2	0.009	1.4 × 10 <sup>16</sup>	1.6 × 10 <sup>15</sup>	4.0 × 10 <sup>11</sup>	9.3 × 10 <sup>12</sup>	2.3 × 10 <sup>13</sup>	4.4 × 10 <sup>16</sup>
D3	0.015	1.4 × 10 <sup>16</sup>	1.6 × 10 <sup>15</sup>	1.0 × 10 <sup>11</sup>	9.3 × 10 <sup>12</sup>	8.6 × 10 <sup>13</sup>	4.4 × 10 <sup>16</sup>
D4	0.028	1.4 × 10 <sup>16</sup>	1.6 × 10 <sup>15</sup>	2.3 × 10 <sup>10</sup>	9.3 × 10 <sup>12</sup>	4.0 × 10 <sup>14</sup>	4.4 × 10 <sup>16</sup>
D5	0.050	1.4 × 10 <sup>16</sup>	1.6 × 10 <sup>15</sup>	7.8 × 10 <sup>9</sup>	9.3 × 10 <sup>12</sup>	1.2 × 10 <sup>15</sup>	4.4 × 10 <sup>16</sup>
D6	0.012	1.4 × 10 <sup>16</sup>	1.6 × 10 <sup>15</sup>	2.7 × 10 <sup>9</sup>	9.3 × 10 <sup>12</sup>	3.4 × 10 <sup>15</sup>	4.4 × 10 <sup>16</sup>
Ar Variation							
E1	0.038	3.0 × 10 <sup>16</sup>	2.2 × 10 <sup>15</sup>	6.4 × 10 <sup>10</sup>	1.3 × 10 <sup>13</sup>	2.7 × 10 <sup>14</sup>	9.8 × 10 <sup>16</sup>
E2	0.043	3.0 × 10 <sup>16</sup>	2.3 × 10 <sup>15</sup>	7.0 × 10 <sup>10</sup>	1.3 × 10 <sup>13</sup>	2.8 × 10 <sup>14</sup>	3.2 × 10 <sup>16</sup>
E3	0.043	3.0 × 10 <sup>16</sup>	2.3 × 10 <sup>15</sup>	7.0 × 10 <sup>10</sup>	1.3 × 10 <sup>13</sup>	2.8 × 10 <sup>14</sup>	1.5 × 10 <sup>16</sup>
E4	0.040	3.4 × 10 <sup>16</sup>	2.1 × 10 <sup>15</sup>	5.9 × 10 <sup>10</sup>	1.4 × 10 <sup>14</sup>	2.9 × 10 <sup>14</sup>	1.3 × 10 <sup>17</sup>

Table 4. Maximum Influence of  $O_2(^1\Sigma) + I_2$  on  $I_2$  Dissociation

Run <sup>a</sup>	$t_{1/2}$ (exp.) (sec)	$t_{1/2}$ (calc.) <sup>b</sup> (sec)	Run <sup>a</sup>	$t_{1/2}$ (exp.) (sec)	$t_{1/2}$ (calc.) <sup>b</sup> (sec)
A1	0.020	0.020	D1	0.002	0.007
A2	0.025	0.023	D2	0.009	0.020
A3	0.034	0.032	D3	0.015	0.027
A4	0.051	0.047	D4	0.028	0.046
A5	0.082	0.070	D5	0.058	> 0.10
A6	0.156	0.125	D6	~ 0.12	> 0.15
B1	0.047	0.052	E1	0.038	0.029
B2	0.068	0.065	E2	0.043	0.029
B3	0.094	0.080	E3	0.043	0.029
B4	0.12	0.090	E4	0.040	0.029
B5	0.165	0.11			
B6	0.25	0.12			
C1	0.026	0.021			
C2	0.016	0.023			
C3	0.012	0.025			
C4	0.0085	0.026			
C5	0.029	0.021			

<sup>a</sup>Table 3

<sup>b</sup>Table 1, except that  $k_5 = k_6 = 0$  and  $k_{1a} = 3 \times 10^{-10}$  cm<sup>3</sup>/molecule-sec.

involving only  $O_2(^1\Delta)$ , i.e.,  $k_5$  and  $k_6$ . The rate of dissociation can thus be increased at the expense of losing the characteristic induction time of the process. The term  $K_{SQ}(1)$  may be important, but the term  $K_{SQ}(2)$  is vastly more important to fitting the shape as well as the  $t_{1/2}$  of the  $I_2$  dissociation curves.

#### B. EXTENT OF $I_2$ DISSOCIATION IN STEADY STATE

The simplified model represented in Table 2 does not include I-atom recombination, so it will not account for incomplete dissociation in steady state. When I-atom recombination is treated in Appendix B, we find that the steady-state amount of  $I_2$  is given by Eq. (B5):

$$[I_2]_{\infty} = -\beta \approx k_{13}/b$$

if  $a_{SQ} + a_z > k_{13}$ . Thus, the I-atom wall recombination coefficient is a potential source of systematic error, because it may vary from experiment to experiment (or even during an experiment) as the walls age.

#### C. $I_2$ DISSOCIATION HALF-LIFE AND EXTENT OF DISSOCIATION: VARIATION WITH INITIAL CONDITIONS (TABLE 3)

##### 1. VARIATION OF $t_{1/2}$ WITH $O_2(^1\Delta)$

An examination of Eq. (19) reveals that the principal dependence of  $t_{1/2}$  on  $[^1\Delta]$  occurs in the denominator term  $a$ . This term is dissected in detail in Table 2. There are implicit dependences on  $[^1\Delta]$  in the term  $c'$  (in  $X$  and  $R_{I_2}^\ddagger$ ); however, these weak dependences are further mitigated by their presence in the logarithmic factor. The same logic applied to the more general Eq. (B7) identifies the critical term as  $\sqrt{-Q}$ . Table 2 indicates that if the subterm  $a_z$  dominates,  $t_{1/2}$  is proportional to  $[^1\Delta]^2$ . If  $a_{SQ}$  dominates, the dependence will fall between  $[^1\Delta]^1$  and  $[^1\Delta]^2$  depending on whether  $R_{I_2}^\ddagger$  is proportional to  $[^1\Delta]$ . Figure 7 shows plots of  $[I_2]$  versus time as  $[^1\Delta]_0$  is varied with all other conditions held constant. Figure 8 summarizes these data as a plot of  $\log t_{1/2}$  versus  $\log [^1\Delta]$ . Within experimental error, the slope is -2 rather than -1, which indicates that  $R_{I_2}^\ddagger$  is a weak function of  $[^1\Delta]$  in this concentration range. We demonstrate that  $a_{SQ} > a_z$  later in this

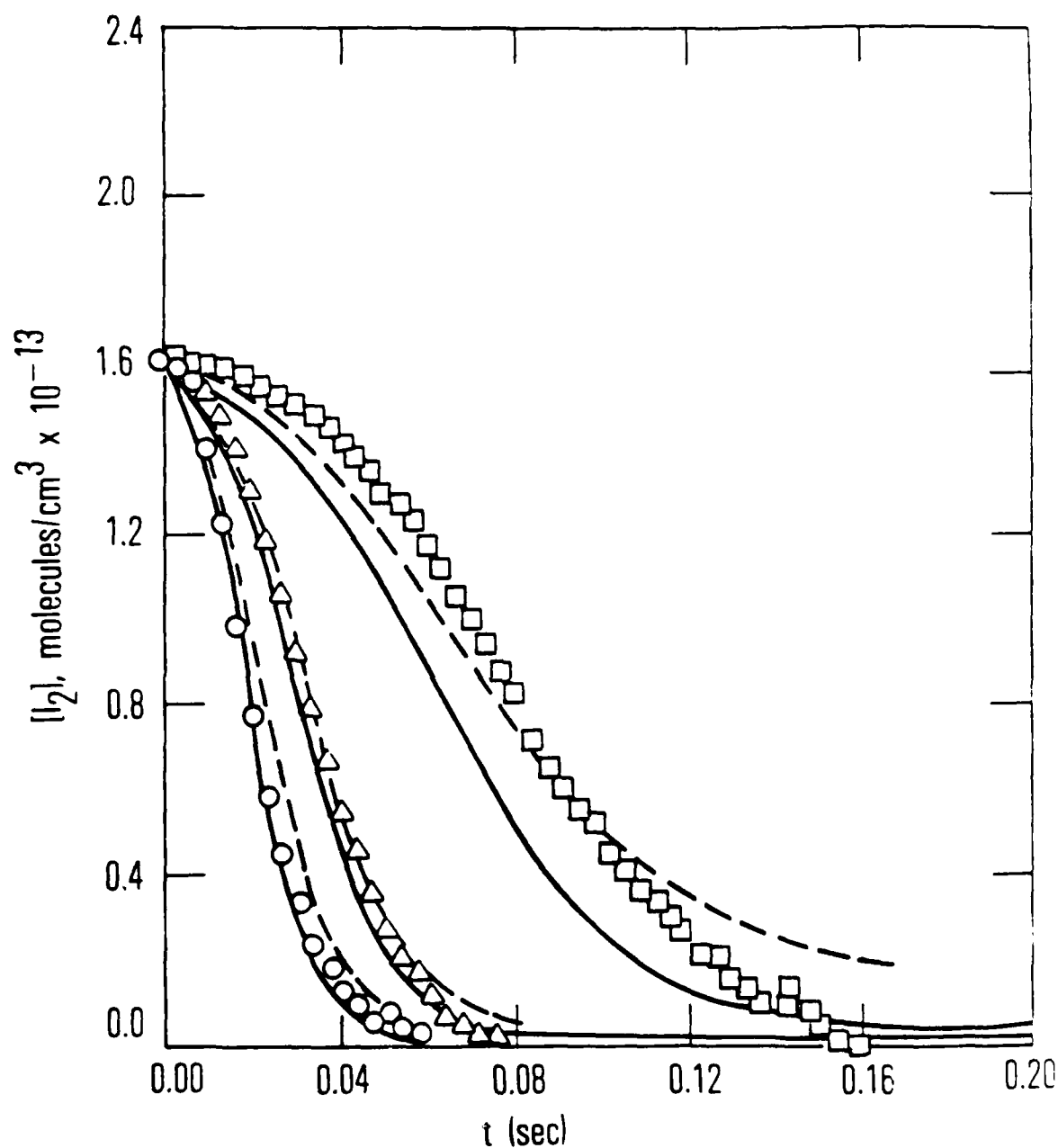


Fig. 7. Experimental Data [Table 3: Runs A1(O), A3( $\Delta$ ), and A5( $\square$ )], Analytic Model Fits (—), and Numerical Model Fits (---) for  $I_2$  Dissociation Versus Time as a Function of  $[I_2]_0$ .

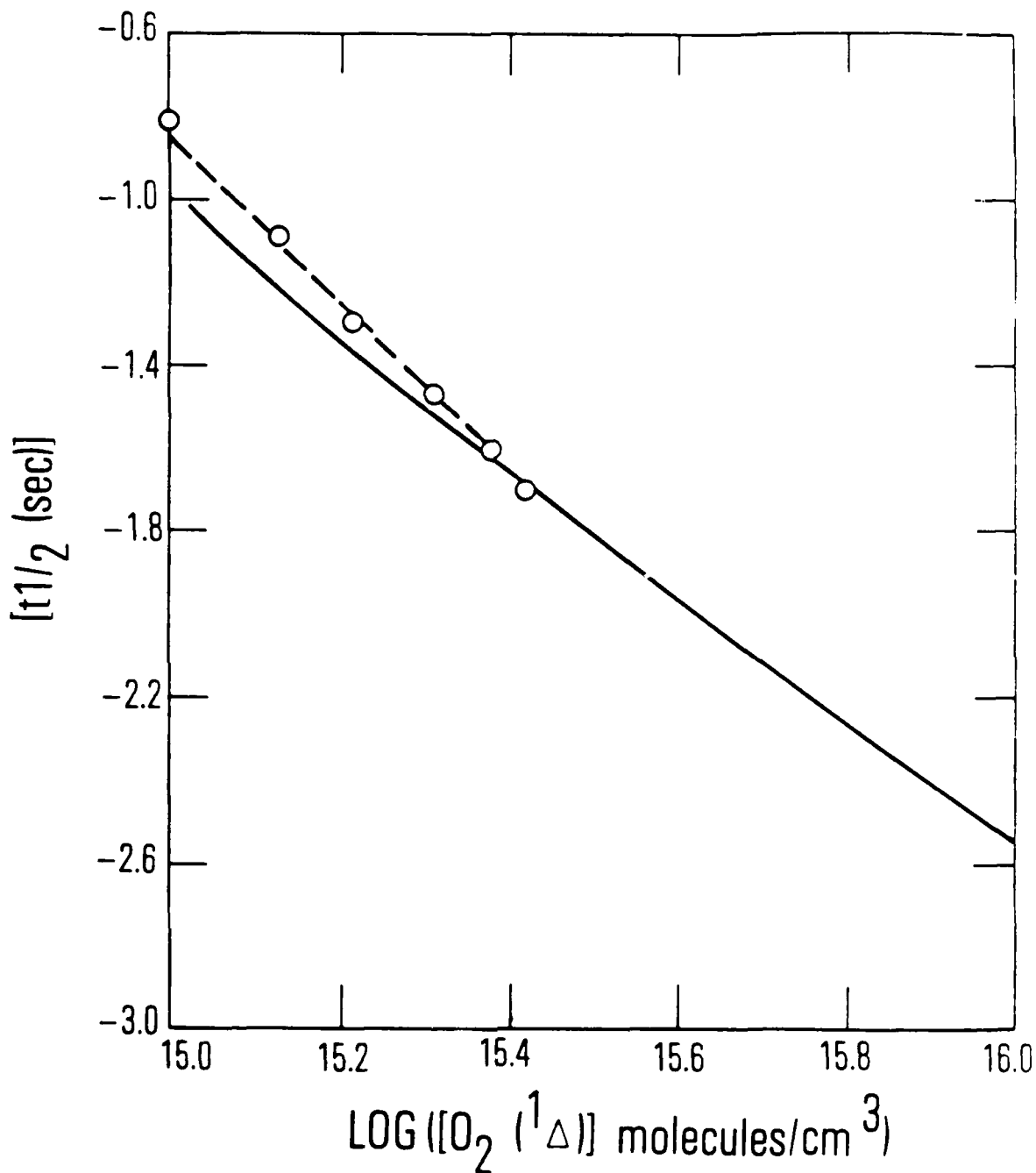


Fig. 8. Plots of Log  $t_{1/2}$  Versus Log  $[^1\Delta]_0$ . Experimental data (O), analytic fits (-), numerical fits (---). Modeling data from Tables 1 and 5.

section. We will examine this dependence on  $^1\Delta$  in detail, because it implies that most of the  $I_2^+$  molecules are not removed by Processes (6) and (8). If the dominant  $I_2^+$  removal process is a quenching process other than Process (-5), serious implications arise for loss of available  $O_2(^1\Delta)$  because of the inefficiency of the dissociation process. This issue is discussed within the context of the measured  $[^1\Delta]$  time profiles during  $I_2$  dissociation. The data in Figures 7 and 8 are fit using empirically determined parameters for  $K_{SQ}(1)$ ,  $K_{SQ}(2)$ , and  $k_{13}$  (Tables 1 and 5).

## 2. VARIATION OF $t_{1/2}$ WITH $O_2(^3\Sigma)$

Equation (19) and Table 2 show an explicit dependence of  $a_2$  on  $[^3\Sigma]^{-1}$ . If  $R_{I_2^+}$  were proportional to  $[^3\Sigma]$ ,  $t_{1/2}$  would be expected to be proportional to  $[^3\Sigma]^2$ . In our experiments,  $X < 0.3$ , so that the term  $c'$  is almost proportional to  $[^3\Sigma]$  ( $\rho$  is concentration independent to first order). Thus, we expect that  $t_{1/2}$  is proportional to  $[^3\Sigma]^n \ln(2 + c''[^3\Sigma]^{-1})$ , where  $c''$  is a constant and  $1 < n < 2$ . Figure 9 shows several plots of  $[I_2]$  versus time with  $[^3\Sigma]$  as a variable. Figure 10 consolidates these results into a  $\log t_{1/2}$  versus  $\log [^3\Sigma]$  plot. A serious ambiguity in these data results because total pressure is held constant by replacing  $O_2(^3\Sigma)$  with Ar. This ambiguity was removed by studying the dissociation time as a function of  $[Ar]$  (Section IV.C.5).

## 3. VARIATION OF $t_{1/2}$ WITH $[I_2]_0$

Analysis of Eq. (19) and Table 2 indicates that the predicted behavior of  $t_{1/2}$  with  $[I_2]_0$  can be quite complicated. The decay curves shown in Fig. 11 point to a dissociation half-life that becomes shorter as  $[I_2]_0$  is increased (Fig. 12). This is the single strongest argument for  $I^*$  participation in the dissociation process. If  $a_2 > a_1$  and  $[I_2]_0/c' \gg 2$ , Eq. (19) predicts that  $t_{1/2}$  is proportional to  $[I_2]_0^{-1} \ln([I_2]_0/c')$ . The slope of  $t_{1/2}$  versus this quantity on a log-log plot is not constant; however, it is given by  $S = -(0.7 \pm 0.1)$  over a wide range of  $[I_2]_0$  if  $c'$  is chosen in a reasonable manner. This dependence occurs using either the  $O_2(^1\Sigma)$  model  $[K_\Sigma(2)]$  or the sequential model  $[K_{SQ}(2)]$  contributions to  $a_2$ . We can quantify  $K_\Sigma(2)$ , however, and



Table 5. Rate Coefficients for the Chain-Reaction Model

A. Sequential Excitation Parameters <sup>b</sup>		Model 1 <sup>c</sup>	Model 2 <sup>c</sup>
$k_5k_6/k_{11b}$		$4 \times 10^{-11}$ cm <sup>3</sup> /molecule-sec	$4 \times 10^{-11}$ cm <sup>3</sup> /molecule-sec
$(k_6k_7 + k_5k_8)/k_{11b}$		$2.2 \times 10^{-10}$ cm <sup>3</sup> /molecule-sec	$2.2 \times 10^{-10}$ cm <sup>3</sup> /molecule-sec
$k_{11a}/k_{11b}$		6	60
$k_{11c}/k_{11b}$		0.06	$2 \times 10^{-3}$

B. Recommended Rate Coefficients <sup>d</sup> Process	k (cm <sup>3</sup> /molecule-sec)	
	Model 1	Model 2
(5)	$7 \times 10^{-15}$ (e)	$7 \times 10^{-15}$ (e)
(-5)	not determined	not determined
(6)	$3 \times 10^{-10}$ (f)	$3 \times 10^{-11}$ (f)
(8)	not determined	not determined
(11a)	$3 \times 10^{-10}$	$3 \times 10^{-10}$
(11b)	$5 \times 10^{-11}$ (f)	$5 \times 10^{-12}$ (f)
(11c)	$4 \times 10^{-12}$	$1 \times 10^{-14}$
(12)	not determined	not determined
(13)	1 sec <sup>-1</sup>	1 sec <sup>-1</sup>

<sup>a</sup>These rate coefficients supplement the literature data in Table 1.

$$R_{I_2} = k_{11b} ([O_2(^3\Sigma)] + (k_{11a}/k_{11b}) [H_2O] + (k_{11c}/k_{11b}) [Ar])$$

$$= k_{11b} X D$$

$$K_{SQ}(1) \text{ (Table 2)} = (k_5k_6/k_{11b}) T^{-1}$$

$$K_{SQ}(2) \text{ (Table 2)} = [(k_6k_7 + k_5k_8)/k_{11b}] T^{-1}$$

<sup>c</sup>Model 2 fits the data in Table 3 somewhat better than Model 1.

<sup>d</sup>These rate packages are consistent with the sequential excitation parameters, but they are not uniquely determined.

<sup>e</sup> $k_6k_7 \gg k_5k_8$ ; therefore  $k_5/k_7 = 1.8 \times 10^{-4}$ ; assumes  $k_7 = 3.5 \times 10^{-11}$  cm<sup>3</sup>/molecule-sec (Table 1).

<sup>f</sup>Assuming  $k_7 = 3.5 \times 10^{-11}$  cm<sup>3</sup>/molecule-sec,  $k_6/k_{11b} = 6$ .

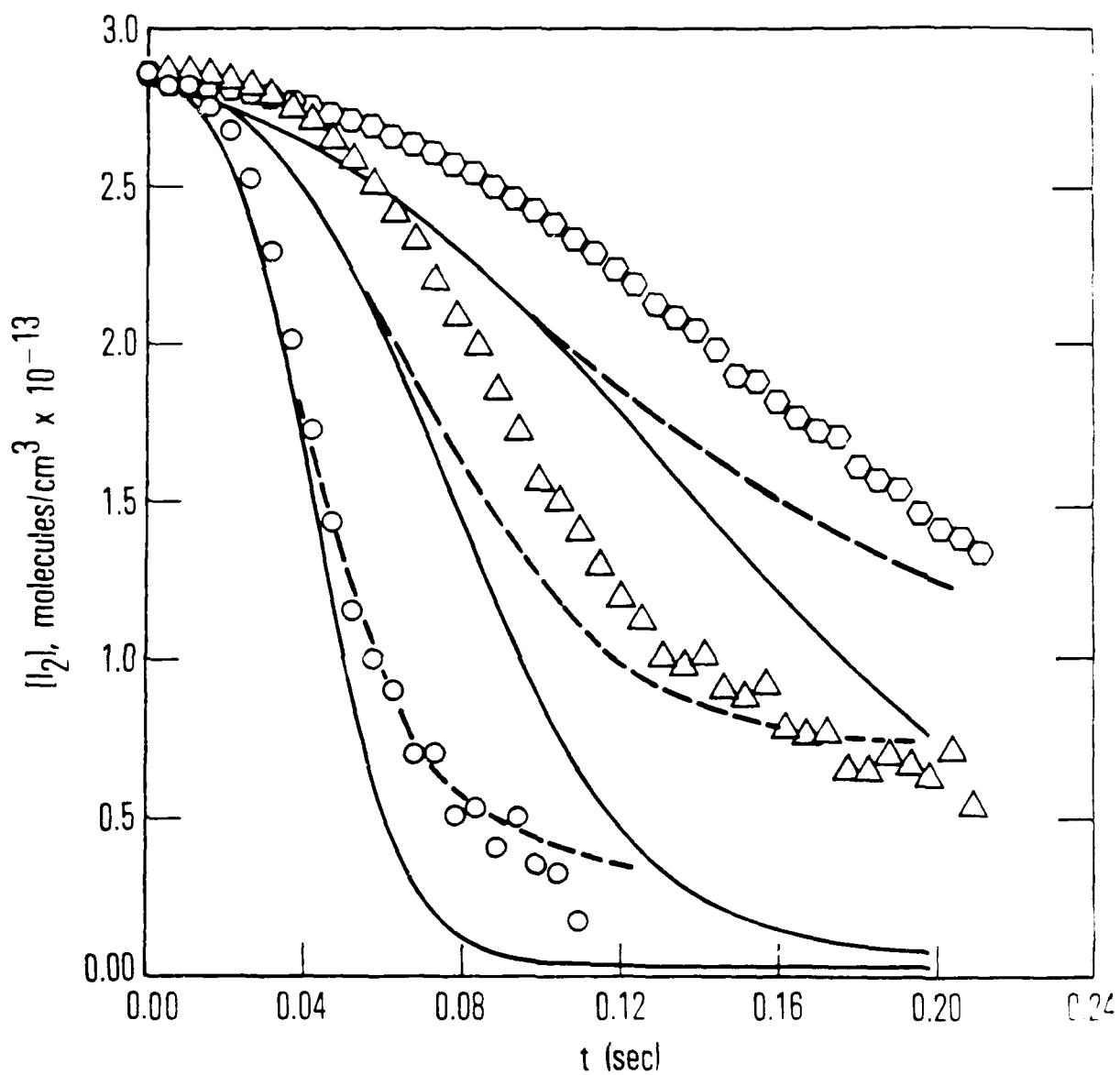


Fig. 9. Experimental Data [Table 3: Runs B1(O), B3( $\Delta$ ), and B5( $\circ$ )], Analytic Model Fits (-), and Numerical Model Fits (---) for  $I_2$  Dissociation Versus Time as a Function of  $[^3Z]_0$ .

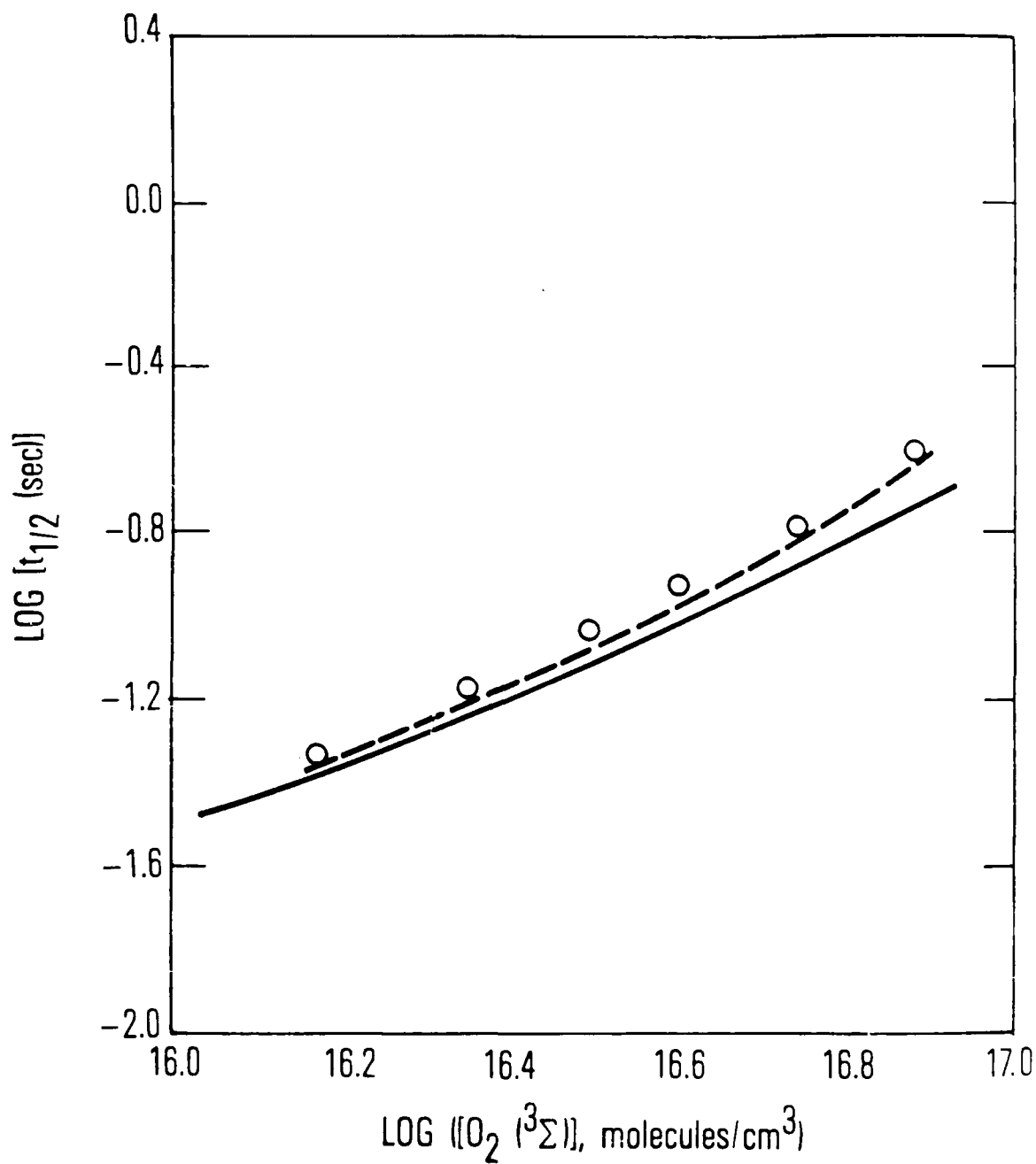


Fig. 10. Plots of  $\text{Log } t_{1/2}$  Versus  $\text{Log } [^3\Sigma]_0$ . Experimental data (O), analytic fits (-), numerical fits (---). Modeling data from Tables 1 and 5.

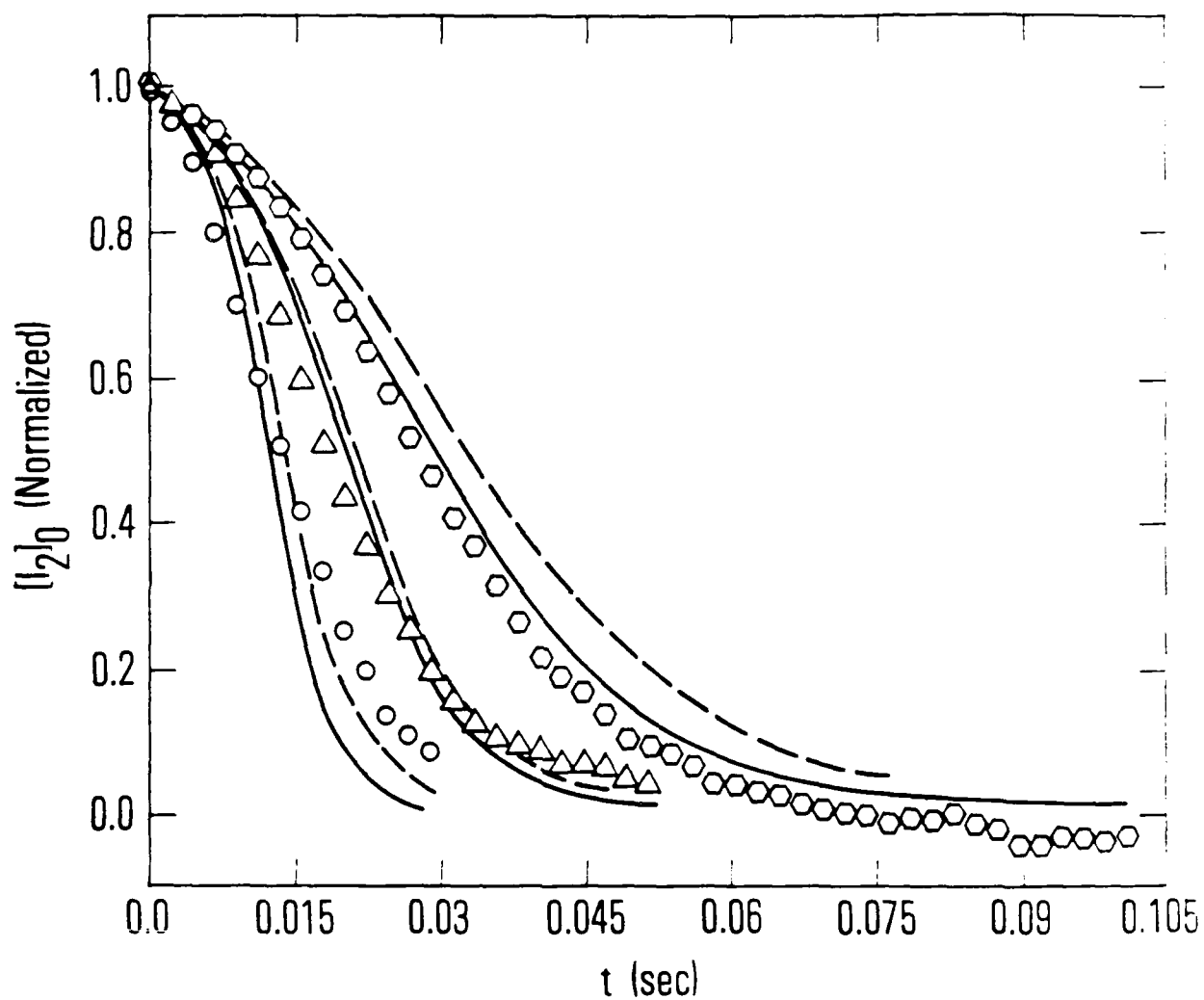


Fig. 11. Experimental Data [Table 3: Runs C3( $\circ$ ), C2( $\Delta$ ), and C1( $\circ$ )], Analytic Model Fits (—), and Numerical Model Fits (---) for  $I_2$  Dissociation Versus Time as a Function of  $[I_2]_0$ .

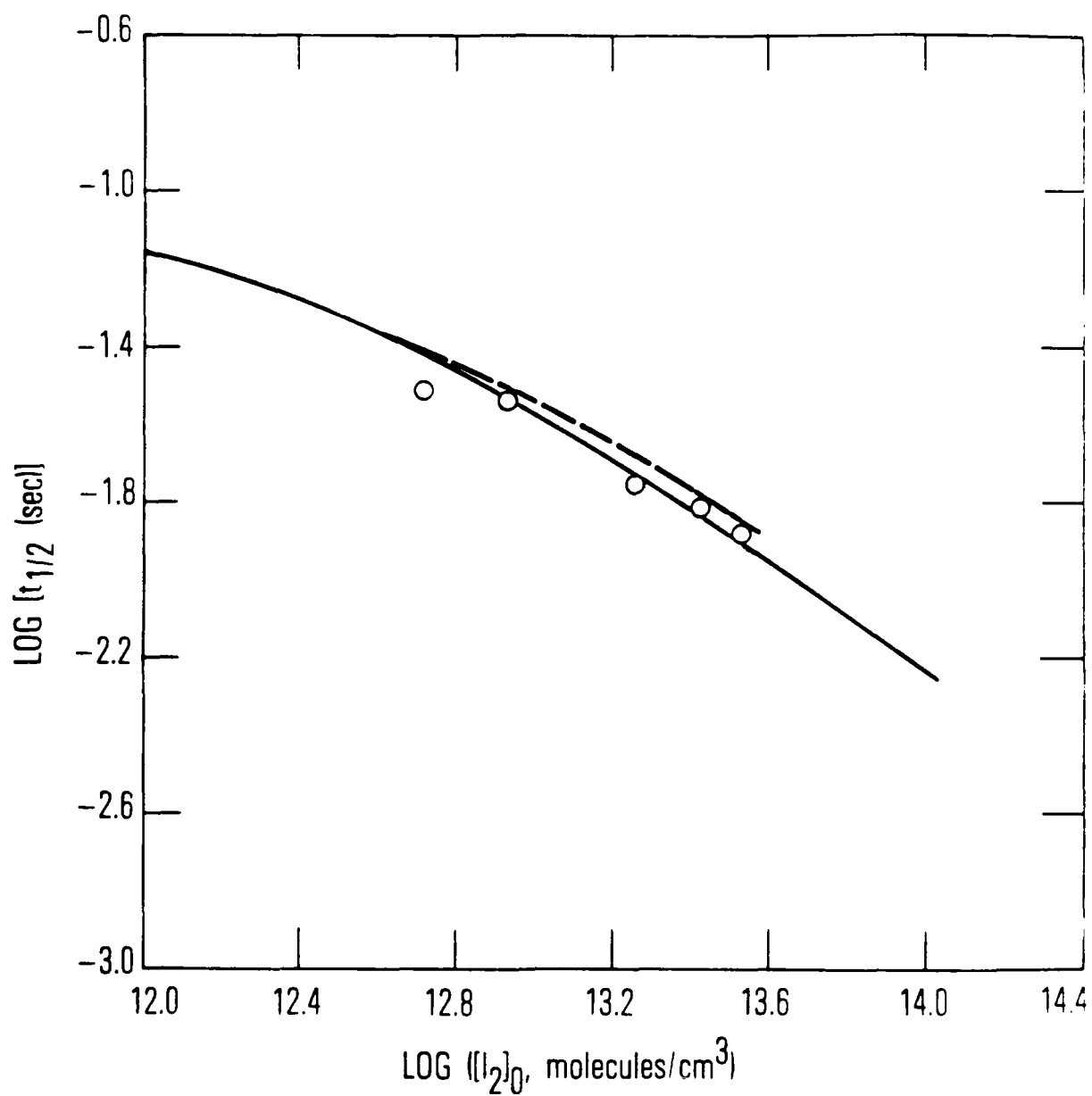


Fig. 12. Plots of  $\text{Log } t_{1/2}$  Versus  $\text{Log } [I_2]_0$ . Experimental data (O), analytic fits (-), numerical fits (---). Modeling data from Tables 1 and 5.

demonstrate with the use of currently accepted values of  $k_{1a}$ ,  $k_3$ , and  $k_9$  that the term  $a_2 \gg a_2$ .

#### 4. VARIATION OF $t_{1/2}$ WITH $H_2O$

The variation of  $t_{1/2}$  with small quantities of  $H_2O$  is discussed in Section IV.A. In addition to effects traceable to  $O_2(^1\Delta)$ , there seems to be a secondary effect at high  $H_2O$  additions that can most easily be explained as a contribution to  $R_{I_2}^{\ddagger}$ . Since  $k_1/k_9 \approx 4$ , the analytic model presented in Section III is valid only for  $[H_2O] \gg 4 [I_2]_0$ . For the data presented in Figs. 13 and 14, this implies  $[H_2O] > 10^{14}/\text{cm}^3$ . We have chosen a value for  $k_{11a}$  to fit the high  $[H_2O]$  data points and then used The Aerospace Corporation numerical modeling code (NEST)<sup>18</sup> to solve for the exact time dependence of  $I_2$  dissociation over the full  $[H_2O]$  range. These calculations are shown in Fig. 14. These fits are less than satisfactory. The fault may be with the model, particularly with the competition between  $I_2$  and  $H_2O$  for  $O_2(^1\Sigma)$ , or it may be in the data themselves. These data were obtained with a very low  $[I_2]_0$  in order to avoid  $O_2(^1\Delta)$  deactivation caused by  $I^* + H_2O$ . Data taken at high  $[I_2]_0$  and at  $[H_2O] \approx 0$  are consistent with Model 2 (Table 5).

#### 5. VARIATION OF $t_{1/2}$ WITH $[Ar]$

The density of Ar was varied over an order of magnitude while a constant initial density of all other species was maintained (Table 3). Within experimental error, we found no dependence of the dissociation rate on Ar (Fig. 15). Figure 16 shows a  $\log t_{1/2}$  versus  $\log [Ar]$  plot. The solid line represents the largest value of  $k_{11c}$  consistent with our observations. Note that the lack of an Ar pressure dependence is unexpected for a vibrationally excited  $I_2^{\ddagger}$  intermediate, but is consistent with the  $O_2(^1\Sigma)$  mechanism. The low contrast ratio of  $[Ar]/[O_2]$  that was experimentally possible does not rule out a vibrationally excited  $I_2$  intermediate if  $O_2$  is a particularly efficient vibrational quencher.

<sup>18</sup>E. B. Turner, G. Emanuel, and R. L. Wilkins, The NEST Chemistry Computer Program, TR-0059(6240-20)-1. The Aerospace Corporation, El Segundo, California, 1970.

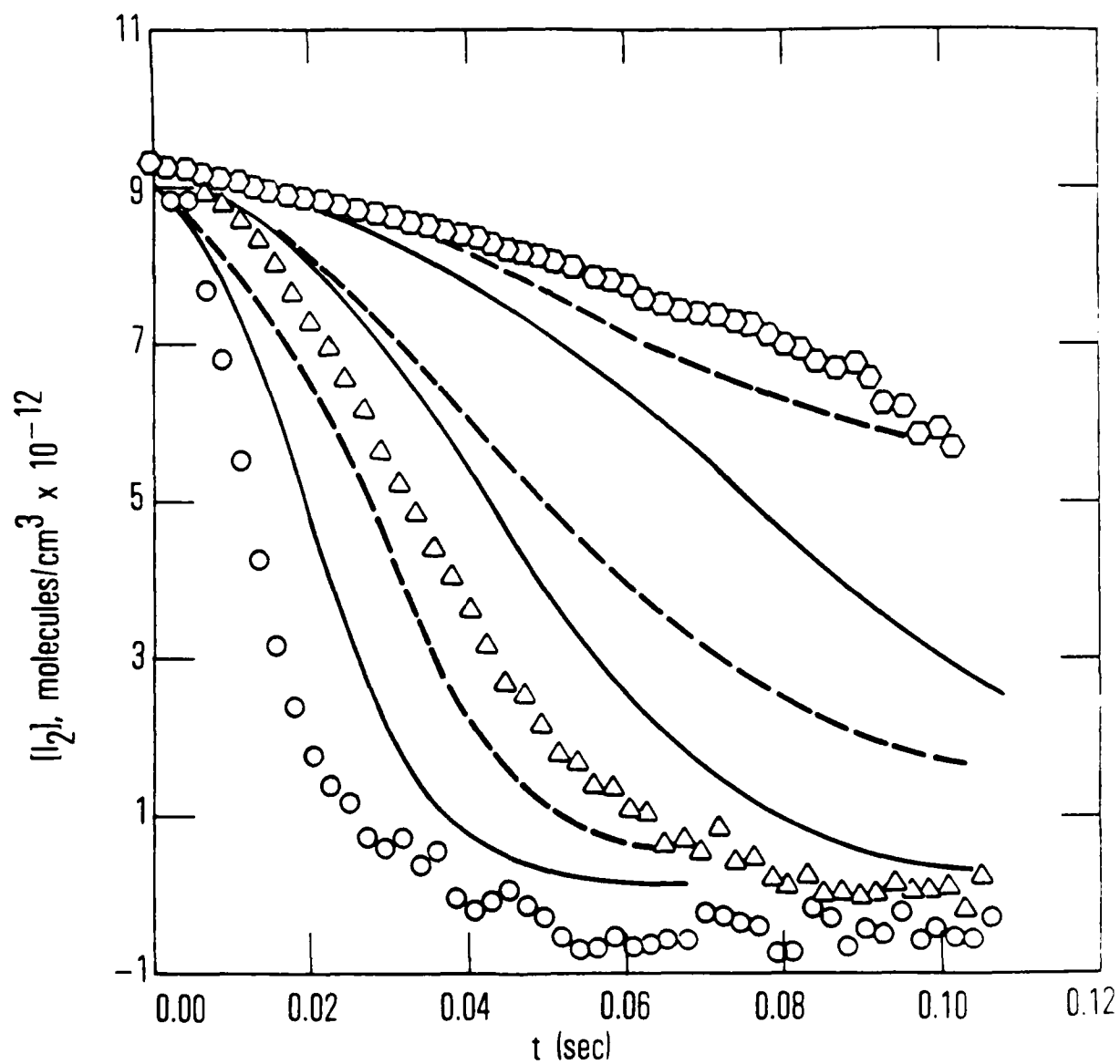


Fig. 13. Experimental Data [Table 3: Runs D2(O), D4( $\Delta$ ), and D6(O)], Analytic Fits (-), Numerical Fits (---) for  $I_2$  Dissociation Versus Time as a Function of  $[H_2O]$ .

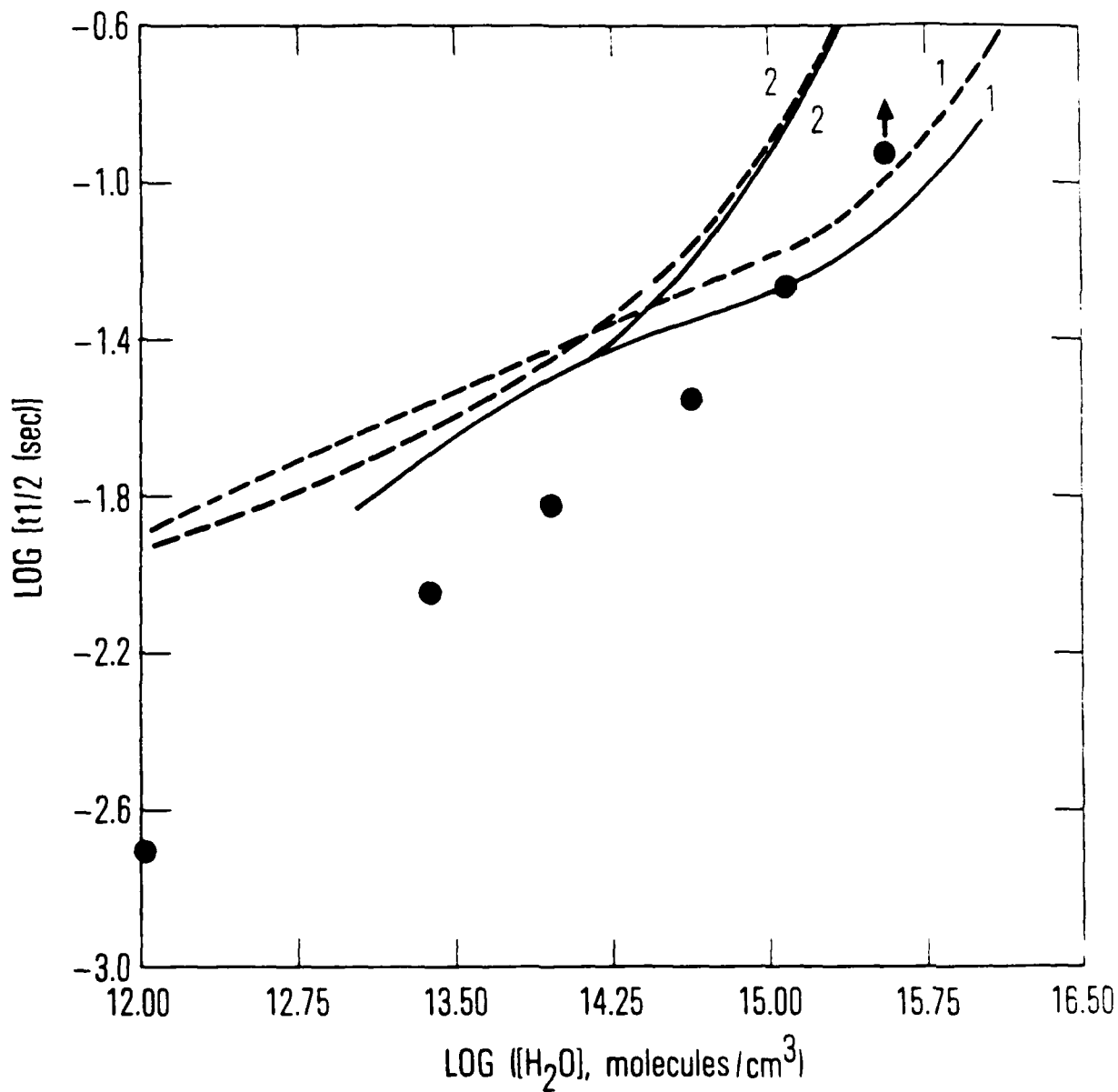


Fig. 14. Plots of  $\text{Log } t_{1/2}$  Versus  $\text{Log } [H_2O]_0$ . Experimental data (O), analytic fits (-), numerical fits (---). Modeling data from Tables 1 and 5. Curves 1 and 2 refer to Models 1 and 2 in Table 5.



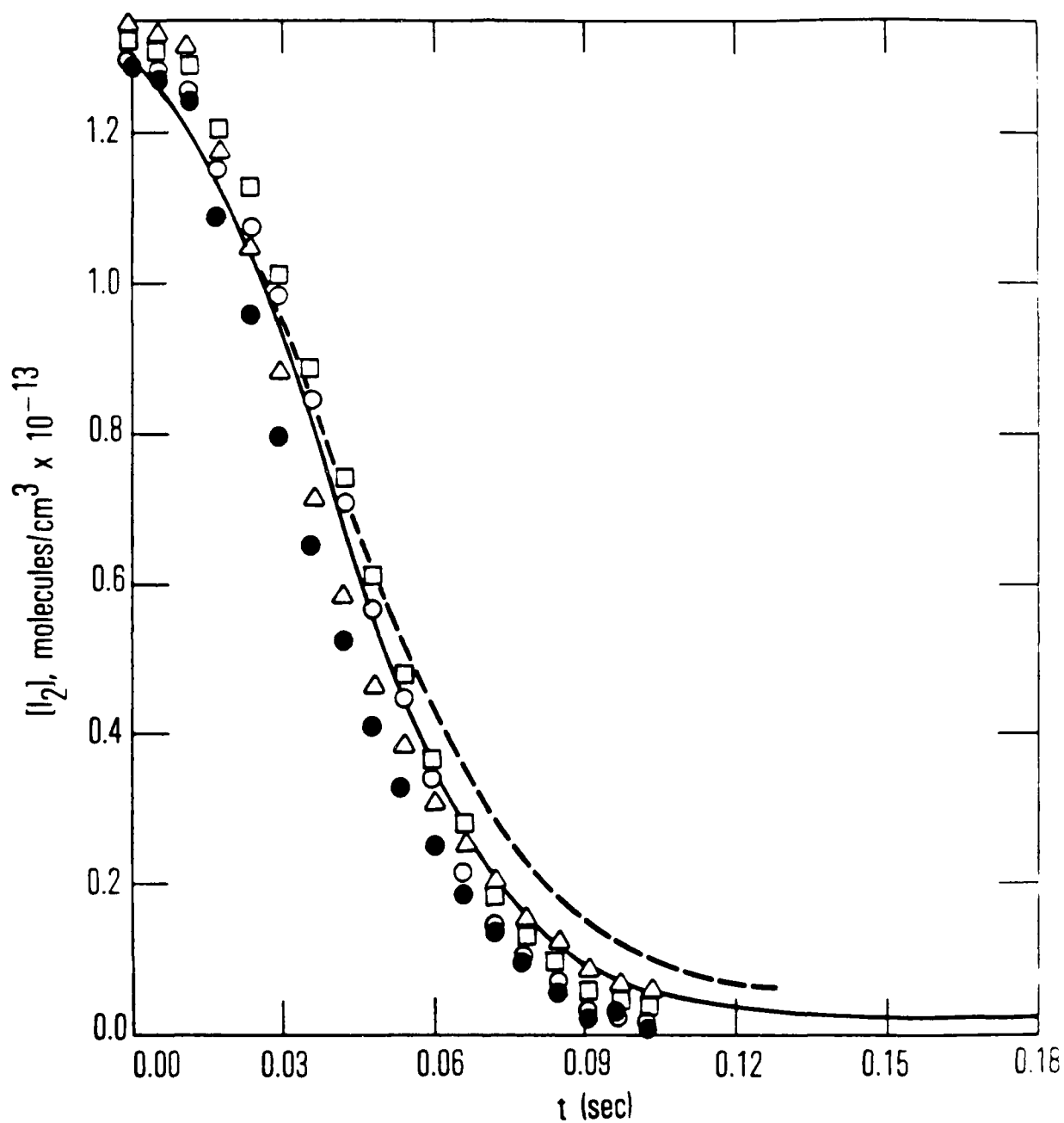


Fig. 15. Experimental Data [Table 3: Runs E1 (●), E2 (□), E3 (○); E4 (Δ)], Analytic Fit (to Run E1) (—), Numerical Fit (to Run E1) (---) for  $I_2$  Dissociation Versus Time as a Function of  $[Ar]$ .

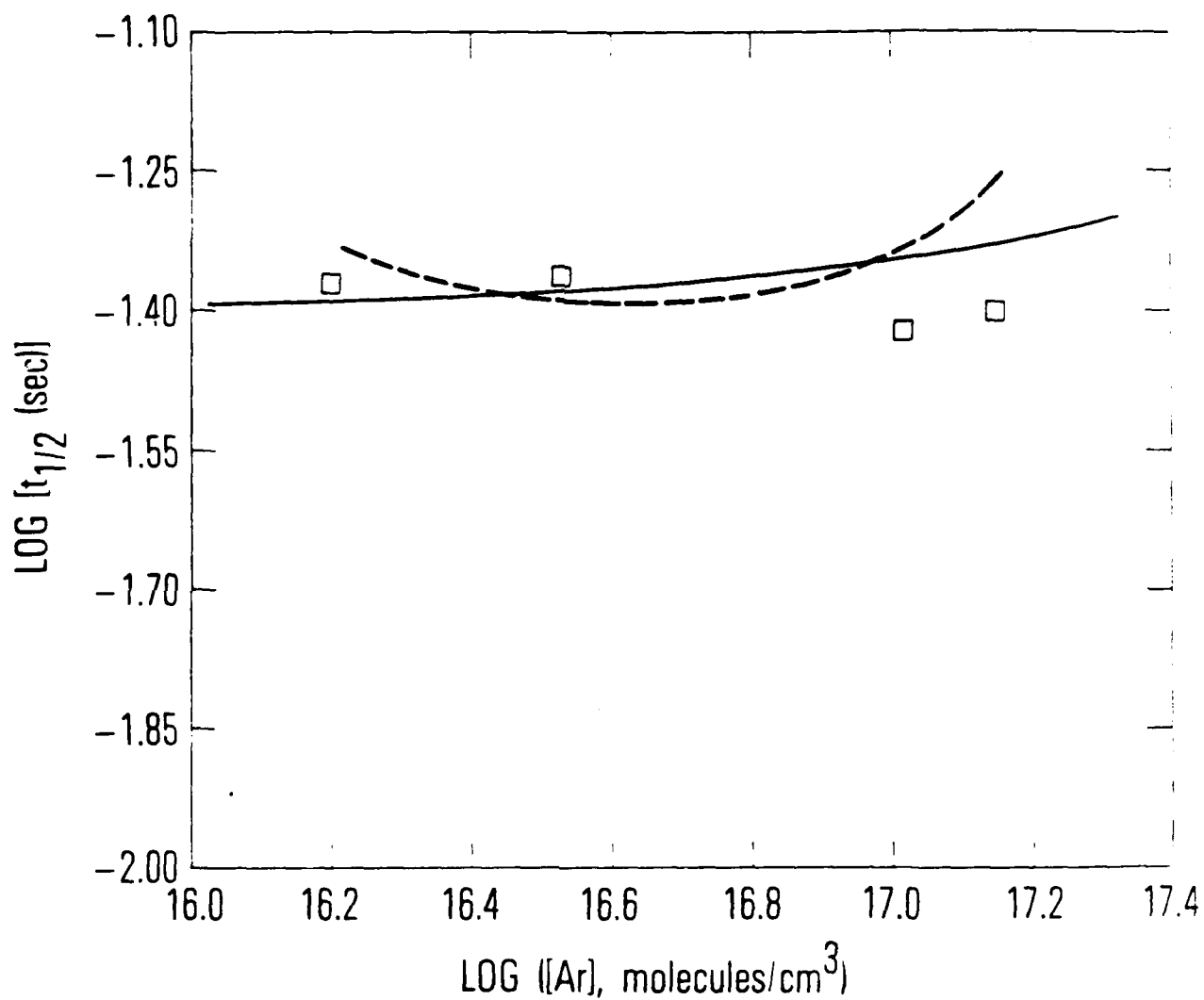


Fig. 16. Plots of  $\text{Log } t_{1/2}$  Versus  $\text{Log [Ar]}$ . Experimental data ( $\square$ ), analytical fit ( $-$ ), numerical fit ( $---$ ). Modeling data from Tables 1 and 5.

## 6. OVERVIEW OF THE $t_{1/2}$ VERSUS $[C_i]$ DATA

The analytic fits to the two types of plots presented, i.e., plots of  $\log t_{1/2}$  versus  $\log [C_i]$  and  $[I_2]$  versus time have identified the variables  $k_{12}$  and  $K_{SQ}(2) [\equiv (k_5 k_8 + k_6 k_7)/R_{I_2^\ddagger}]$  as critical. Somewhat less important for the concentration ranges studied are the variables  $K_{SQ}(1) [\equiv (k_5 k_6)/R_{I_2^\ddagger}]$  and  $k_{1a}$ . The detailed analysis of  $K_{SQ}(2)$  presents a number of problems:

1. What is  $I_2^\ddagger$ ?
2. What are the important contributions to  $R_{I_2^\ddagger}$ ?
3. What are the absolute magnitudes of  $R_{I_2^\ddagger}$  and  $(k_5 k_8 + k_6 k_7)$ ?

Numerous workers in this field, including the present authors, have suggested that there are two major possibilities for the identity of  $I_2^\ddagger$ . As suggested by Ogryzlo and coworkers,<sup>1</sup> the intermediate could be  $I_2(A'^3\Pi_{2u})$ . The other possibility for the intermediate is vibrationally excited  $I_2$ .<sup>19-21</sup> Neither of these explanations is immune to criticism.

In an earlier paper on  $I_2$  dissociation,<sup>14</sup> we reiterated the suggestion that  $I_2(A'^3\Pi_{2u})$  could be the product of Process (5) and/or (7). Recently published spectroscopic analysis<sup>19</sup> has identified this state as the lower level of the  $I_2$  laser at 3400 Å ( $D' \rightarrow A'$ ). Tellinghuisen and Wieland<sup>19</sup> have argued that the total of the spectroscopic data requires a  $T_e$  value for  $A'^3\Pi_{2u}$  of 10,047.5  $\text{cm}^{-1}$ . Independent measurements by Koffend et al.<sup>22</sup> confirm this position for  $A'$ . Thus, Process (5) would appear to be  $\sim 2060 \text{ cm}^{-1}$  endoergic and Process (7) would be  $\sim 2340 \text{ cm}^{-1}$  endoergic. At  $T = 295 \text{ K}$ , these processes could not occur rapidly enough to avoid limiting the rate of  $I_2$  dissociation in an unrealistic fashion. If  $I_2^\ddagger$  denotes vibrationally excited  $I_2$ , we must assume that vibrational relaxation is rapid, although some relaxation could be tolerated and  $I_2^\ddagger$  would still have sufficient energy for Process (6) to be energetically feasible. If this were the case,  $R_{I_2^\ddagger}$  would

<sup>19</sup>J. Tellinghuisen and K. Wieland, J. Mol. Spectrosc, to be published.

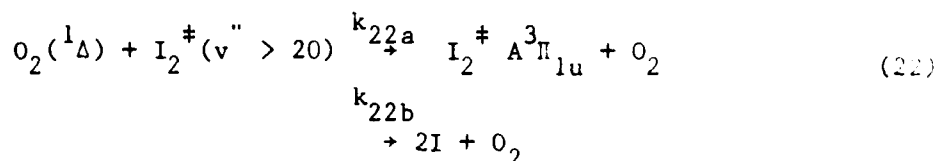
<sup>20</sup>G. Black, private communication (1980).

<sup>21</sup>P. L. Houston, private communication (1981).

<sup>22</sup>J. B. Koffend, R. Bacis, and A. Sebail, to be published (1982).

be very large and  $k_6$  must be nearly gas kinetic to permit  $O_2(^1\Delta)$  to compete for  $I_2^\ddagger$ . On the other hand,  $k_6[{}^1\Delta]$  cannot dominate  $R_{I_2^\ddagger}$  completely without producing a  $[{}^1\Delta]^{-1}$  dependence of  $t_{1/2}$  instead of the observed  $[{}^1\Delta]^{-2}$ .

If we accept that  $R_{I_2^\ddagger}$  must be large in a vibrationally excited intermediate model, we cannot realistically expect that  $I^*$  participates by energy transfer to  $I_2^\ddagger$ . Thus, Process (8) is much less important than Process (6) in producing  $I$  atoms. Of course if vibrational relaxation is slower than we expect on the basis of the work of Koffend et al.,<sup>23</sup> the reaction sequence ( $k_5$ ,  $k_8$ ) could still be possible. At present, we believe that Process (6) is rapid and that it must therefore proceed on the basis of  $E \rightarrow E$  transfer, most probably



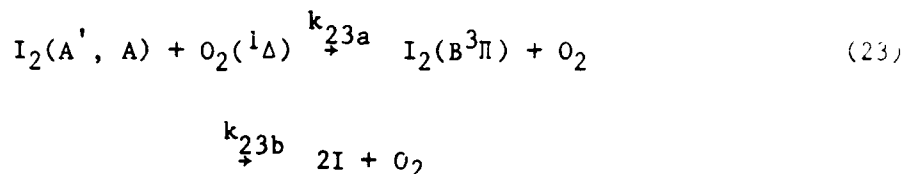
which would account for the observed presence of  $I_2(A^3\Pi_{1u})$  during the dissociation process. If  $I_2^\ddagger$  is vibrationally excited  $I_2$ , increasing the total pressure of buffer gas (with  $[{}^1\Delta]$ ,  $[{}^3\Sigma]$ ,  $[I_2]_0$ , and  $[H_2O]$  constant) should demonstrate some significant effects both on  $t_{1/2}$  and the quantum yield of  $A^3\Pi_{1u}$ . This was not observed (Figs. 15 and 16 and Table 3). Thus, Ar must be significantly less efficient than  $O_2(^3\Sigma)$  or  $H_2O$  as a vibrational relaxer of  $I_2$ .

Pritt<sup>24</sup> has suggested that  $A^3\Pi_{1u}$  and  $A'^3\Pi_{2u}$  may be populated below their dissociation limit by the second step of the sequential transfer and that dissociation may require the participation of a third pump species ( $I^*$  or  ${}^1\Delta$ ). This mechanism would produce dissociation terms that are third-order in  $O_2(^1\Delta)$

<sup>23</sup>J. B. Koffend, F. J. Wodarczyk, R. Bacis, and R. W. Field, J. Chem Phys. 72, 478 (1980).

<sup>24</sup>A. T. Pritt, Jr., private communication (1982).

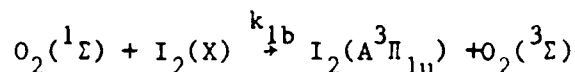
and could permit an observed second-order dependence on  $^1\Delta$  if the final step of the dissociation, i.e.,



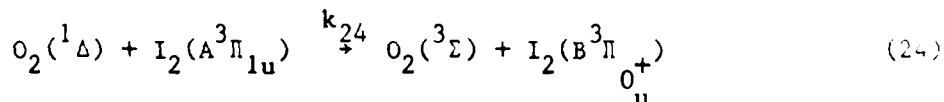
dominates the loss of  $\text{I}_2(\text{A}', \text{A})$ . Several other three step models are capable of demonstrating the correct kinetic order for dissociation.

D. BEHAVIOR OF  $\text{I}_2(\text{A}^3\Pi_{1u})$  AND  $\text{I}_2(\text{B}^3\Pi_{0u}^+)$

In their series of papers on the  $\text{O}_2\text{-I}_2$  system, Derwent and Thrush<sup>2,3,8-10</sup> invoked a mechanism for the  $\text{I}_2(\text{B} + \text{X})$  chemiluminescence that had rather significant mechanistic implications. They postulated that  $\text{I}_2(\text{A}^2\Pi_{1u})$  (which they did not observe) was formed as a major product of Process (1b)



and that  $\text{I}_2(\text{B}^3\Pi)$  was formed by Process (24)



We observed a near-infrared transition analyzed to be  $\text{I}_2(\text{A} + \text{X})$  emission originating from the  $v' = 0$  and 1 levels.<sup>16</sup> Figure 17 shows that the time dependence of both emission bands serves as a useful diagnostic for the dissociation of  $\text{I}_2(\text{X})$ . Qualitatively, the data for these two band systems are consistent with the Derwent and Thrush mechanism. Because the  $\text{A} + \text{X}$  and  $\text{B} + \text{X}$

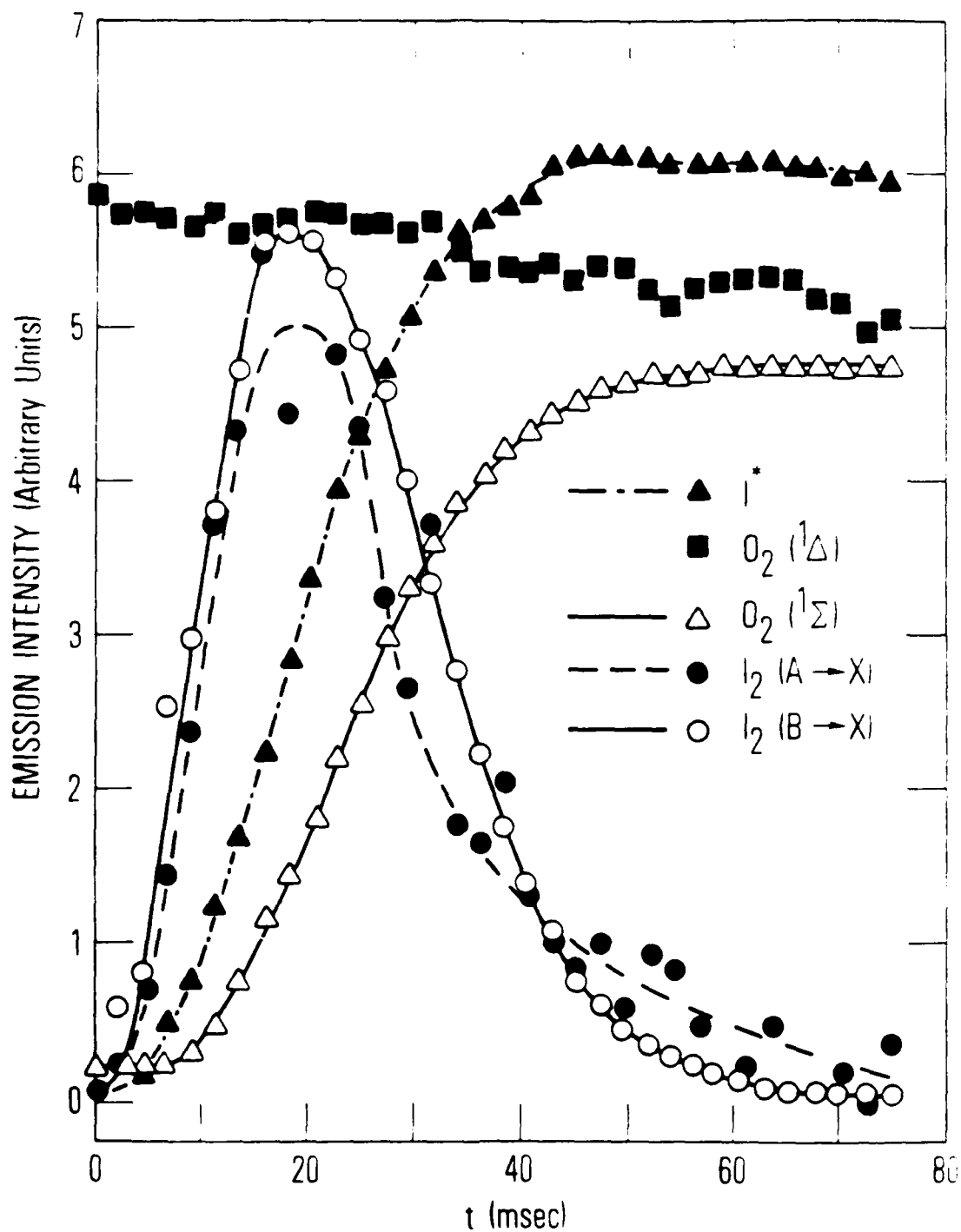


Fig. 17. Time Profiles for  $I_2(A + X)$  and  $I_2(B + X)$  Relative to Other Measured Species. Experimental data: Run D3 (Table 3). The lines are empirical fits rather than theoretical.

emission profiles are similar under all experimental conditions studied, the A and B states either have the same precursor or  $B^3\Pi$  is produced from, and maintains a steady-state relationship to,  $A^3\Pi$ . A simple way to view the traces in Fig. 17 is to analyze Eq. (A4) from Appendix A with  $R_\Sigma$  constant (dominated by  $H_2O$  quenching) and with  $[^1\Delta]$  constant. In that case, the  $[^1\Sigma]_{ss}$  increases linearly with the  $[I^*]$  (see Fig. 17) and the Derwent and Thrush mechanism ( $k_{1b}$ ,  $k_{24}$ )  $A^3\Pi$  and  $B^3\Pi$  concentration dependences can be written as follows:

$$[I_2(A)] = k_A \frac{[I^*] [I_2]}{R_A} \quad (25)$$

where  $R_A$  ( $\text{sec}^{-1}$ ) contains the removal terms for the  $A^3\Pi_{1u}$  state and  $k_A$  is a constant. This analysis assumes  $k_2[^1\Delta] < k_3[I^*]$ . When this simple steady-state analysis is used,  $[I_2(A)]_{\max}$  occurs when  $[I_2]$  has reached half-minimum and  $[I^*]$  has reached half-maximum. If  $[^1\Delta]$  remains constant during the dissociation and  $B^3\Pi$  is in steady state with  $A^3\Pi$ , then

$$[I_2(B)] = k_B \frac{[I_2(A)] [^1\Delta]}{R_B} \quad (26)$$

where  $R_B$  represents the total removal rate of  $B^3\Pi$  state molecules. Thus,  $I_2$  ( $B \rightarrow X$ ) emission has the same temporal profile as  $I_2(A \rightarrow X)$ , but scales differently with the  $[^1\Delta]$ .

This temporal behavior for  $A^3\Pi$  and  $B^3\Pi$  is not unique to the Derwent and Thrush mechanism. The sequential mechanism favored by this study ( $k_7$ ,  $k_6$ ) invokes a vibrationally excited  $I_2(X)$  intermediate. On these flow tube time scales,  $I_2^+$  will be held in steady state by the rapid removal rates,  $R_{I_2^+}$ , that are typical of vibrational relaxation processes in heavy diatomics. Thus, we can write

$$[I_2^+]_{ss} = \frac{k_7}{R_{I_2^+}} [I^*] [I_2] \quad (27a)$$

$$[I_2(A)]_{ss} \approx \kappa_A [I^*] [I_2] \quad (27b)$$

$$[I_2(B)]_{ss} \approx \kappa_B [I^*] [I_2] \quad (27c)$$

where  $\kappa_A = (k_{22a} k_7) / (R_{I_2} + R_A) [^1\Delta]$  and  $\kappa_B = \left( \frac{k_{24} \kappa_A}{R_B} \right) [^1\Delta]$ .

#### E. $I_2$ DISSOCIATION IN AN $H_2O$ -FREE $O_2^*$ SYSTEM

The analytic model presented in this study requires four fundamental assumptions: (1)  $[^1\Delta]$  constant during  $I_2$  dissociation; (2)  $^1\Sigma$  in steady state and  $R_\Sigma$  not a function of  $I_2$ ; (3)  $I_2^{\ddagger}$  in steady state; and (4)  $[I_2^{\ddagger}] \ll [I_2]$ .

Experimental conditions were chosen, as far as feasible, to satisfy these constraints and suppress the role of  $O_2(^1\Sigma)$  as a dissociation initiator by means of Process (1a). It is instructive to remove these constraints in order to study  $I_2$  dissociation under conditions where  $O_2(^1\Sigma)$  is removed either by  $I_2$  or by wall collisions. If we use values of  $k_{10}$  and  $k_2$  from Table 1, the value of  $[^1\Sigma]_0$  at  $I_2$  injection is given by Eq. (A4) or, specifically, by

$$[^1\Sigma]_0 \approx 1 \times 10^{-18} [^1\Delta]_0^2 \quad (28)$$

under  $H_2O$ -free conditions in our apparatus. In this section, the system behavior for various ratios of  $\Theta \equiv [^1\Delta]_0 / [I_2]_0$  is examined. Because  $[^1\Sigma]_0$  can dissociate  $(k_{1a}/k_1) \times [^1\Sigma]_0$  molecules of  $I_2$ , we can approximate the fractional dissociation at  $t = 0$  as follows:

$$F = 1 - [I_2]/[I_2]_0 = 10^{-18} (k_{1a}/k_1) \Theta [^1\Delta]_0 \quad (29)$$

For  $\Theta = 100$ , which is typical both of these experiments and the transfer laser devices,  $k_{1a}/k_1 \approx 0.2$  (Table 1) and  $[^1\Delta] = 2 \times 10^{15}/\text{cm}^3$ ,  $O_2(^1\Sigma)$  is responsible



for  $F = 0.04$ . The fractional dissociation is very sensitive to concentration and rate coefficient values in this regime.

Figure 18a indicates the complexity of the  $I_2$  dissociation curves when  $O_2(^1\Sigma)$  is active during the initiation phase. Initially, the density of  $O_2(^1\Sigma)$  is driven lower by the presence of  $I_2$  as a quencher [Eq. (A4)]. At  $t = 120$  msec, the  $I_2$  has been removed from the system and the  $[^1\Sigma]$  rises rapidly toward a new steady-state value.<sup>4</sup> Qualitatively,  $O_2(^1\Sigma)$  can be viewed as an end-point indicator in an  $I_2$  titration. The peculiar shape of the  $I^*$  rise curve derives from rapid dissociation initiation by  $O(^3P)$  and  $O_2(^1\Sigma)$ . If we use the rate package in Table 1 with no contribution from Process (20), the  $I^*$  rise time is not correctly predicted. A much better fit for  $I^*$  is obtained by using  $[O(^3P)]_0 = 2 \times 10^{12}/\text{cm}^3$ . In both cases, the behavior of  $O_2(^1\Sigma)$  is not quantitatively correct. One must choose between increasing  $k_{1a}$  and/or  $k_{1b}$  in the Table 1 model or postulating additional transient quenchers of  $O_2(^1\Sigma)$  during the  $I_2$  dissociation. The curves in this figure can be considered "well-behaved," in the sense that for  $\Theta = 59$ , dissociation of  $I_2$  is complete with  $< 10\%$  of the  $O_2(^1\Delta)$  removed. The inversion density in the  $O_2(^1\Delta) - I$  atom transfer laser can be written

$$\dot{\rho} = [I^*] - \frac{1}{2} [I] = \left(\frac{2X-1}{X+1}\right) ([I_2]_0 - [I_2]) \quad (30)$$

where  $X = k_{EQ} [^1\Delta]/[^3\Sigma]$ . Clearly,  $\dot{\rho}$  is maximized by large values of  $X$  and large values of  $[I_2]_0 - [I_2]$ .

Figure 18b illustrates the perils of trying to increase  $\dot{\rho}$  by operating at lower values of  $\Theta$ . In this figure,  $\Theta = [^1\Delta]_0/[I_2]_0 = 9$ . In principle, the dissociation rate increases as  $[I_2]_0$  is increased (Fig. 12); however,  $O_2(^1\Delta)$  is being rapidly depleted, which drastically slows the dissociation rate (Fig. 8). The net result is that  $< 40\%$  of the  $I_2$  is dissociated at the peak in the  $I^*$  curve. Model 2 correctly represents the general behavior of  $O_2(^1\Delta)$ ,  $O_2(^1\Sigma)$ , and  $I^*$  under these demanding experimental conditions. The curve for  $I_2^{\ddagger}$  (Model 2) is scaled to the arbitrary height of  $I_2(A)$ . Although the curves

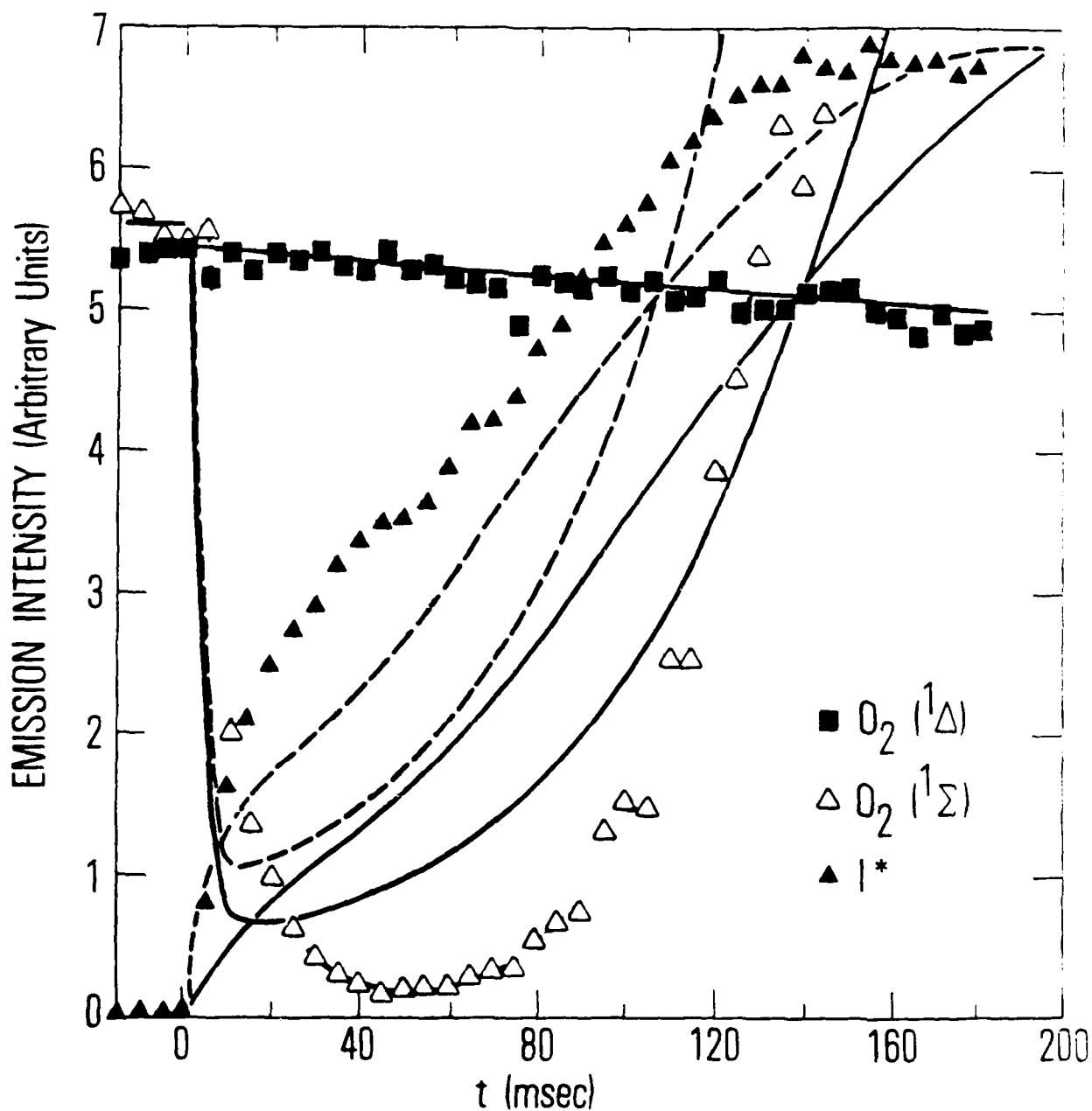


Fig. 18a.  $I_2$  Dissociation in an  $H_2O$ -Free  $O_2^*$  System. (a) Full dissociation, constant  $[^1\Delta]$ ,  $[I_2]_0 = 2.0 \times 10^{13}/\text{cm}^3$ . Model 2 numerical fit to (a) and (b) except for  $I_2(A,B)$ . Other conditions:  $[^1\Delta]_0 = 1.2 \times 10^{15}$ ;  $[^1\Sigma]_0 = 1.4 \times 10^{12}$ ;  $[^3\Sigma] = 7.7 \times 10^{16}$ ;  $[H_2O] = 0$ ;  $[Ar] = 2.0 \times 10^{16}/\text{cm}^3$ ;  $[O(^3P)]_0 = 0$  (—) or  $2 \times 10^{12}$  (---) in (a).

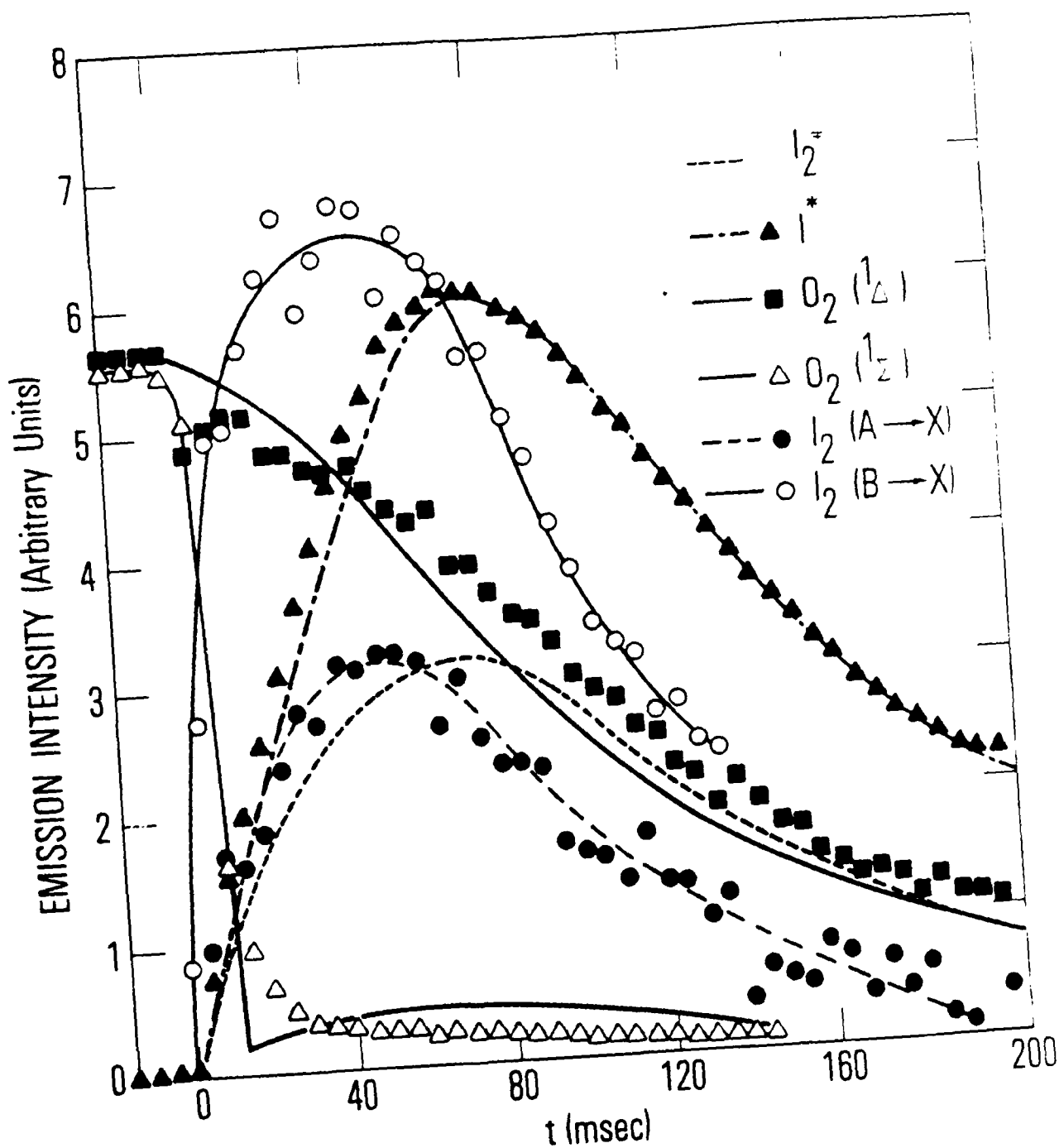


Fig. 18b.  $I_2$  Dissociation in an  $H_2O$ -Free  $O_2^*$  System. (b) Partial dissociation, decaying  $[^1\Delta]$ ,  $[I_2]_0 = 1.3 \times 10^{14}/cm^3$ . Model 2 numerical fit to (a) and (b) except for  $I_2(A,B)$ . Other conditions:  $[^1\Delta]_0 = 1.2 \times 10^{15}$ ;  $[^1\Sigma]_0 = 1.4 \times 10^{12}$ ;  $[^3\Sigma] = 7.7 \times 10^{16}$ ;  $[H_2O] = 0$ ;  $[O(^3P)]_0 = 2.0 \times 10^{16}/cm^3$ ;  $[O(^3P)]_0 = 0$  (—).

are similar, as we demonstrated in Section IV.D, this does not prove that  $I_2(A)$  or  $I_2(A')$  is the intermediate  $I_2^\pm$ . For these low  $\Theta$  values, the efficiency of the dissociation process is crucial. Figure 1 emphasizes that on the basis of energetics alone, two  $O_2(^1\Delta)$  molecules are required to dissociate an  $I_2$  molecule. Within the context of the analytic model, the efficiency of the Derwent and Thrush mechanism,  $E_\Sigma$ , is given by  $E_\Sigma = k_{1a} [I_2]/R_\Sigma$  and that of the sequential model,  $E_{SQ}$ , by  $E_{SQ} = k_6 [^1\Delta]/R_{I_2^\pm}$ . Clearly, if  $\Theta = 10$ ,  $E_{EFF}$  cannot be 0.1 and still yield good laser performance. The presence of large  $I_2(X)$  concentrations in Figure 18b produces good S/N traces for  $I_2(A \rightarrow X)$  and  $I_2(B \rightarrow X)$  over the entire length of the flow tube. It may be possible to derive fine details of the dissociation model by careful studies of these two band systems.

Long-time decay studies of  $O_2(^1\Delta)$  at  $\Theta < 100$  are useful in verifying kinetic parameters for the  $O_2(^1\Delta) - I$  atom system. For example, the removal rate of  $O_2(^1\Delta)$  is predominantly a second-order process at high  $[I^*]$ . The preliminary rate coefficient ( $\sim 2 \times 10^{-13}$  cm<sup>3</sup>/molecule-sec) is consistent with the rate coefficient for the energy pooling process  $k_3$ .

## V. SUMMARY AND CONCLUSIONS

In this study, we have demonstrated that the dissociation of  $I_2$  in electronically excited oxygen can be considered to be a chain reaction. The initiator species in the present discharge flow system were identified as  $O(^3P)$  and  $O_2(^1\Sigma)$ , although large-scale continuous-wave laser systems may initiate the dissociation with other species as well. The chain carrier in the dissociation process was identified as  $I^*$ . In an environment where  $O_2(^1\Sigma)$  is constant,  $I^*$  increases with the extent of  $I_2$  dissociation and thus accelerates the further production of  $I$  atoms by means of processes such as (7) and (8). Sufficient data have been collected to quantify previous observations that the  $O_2(^1\Sigma)$  mechanism was not sufficient to explain the empirical rate of  $I_2$  dissociation.<sup>14</sup> The  $O_2(^1\Sigma)$  mechanism may be necessary for initiating the dissociation under experimental conditions where  $K_\Sigma(1) (\equiv k_{1a}k_2/R_\Sigma)$  proves to be greater than  $K_{SQ}(1) (\equiv k_5k_6/R_{I_2^*})$ . Our flow tube studies indicate that such conditions exist for small  $H_2O$  densities.

The identification of intermediate states in a kinetic mechanism by indirect methods is always unsatisfactory and frequently erroneous. Using the scaling of the dissociation half-life  $t_{1/2}$  with  $O_2(^1\Delta)$ ,  $O_2(^3\Sigma)$ ,  $I_2$ ,  $H_2O$ , and Ar, we formulated the problems created by either of the two sequential mechanisms considered. The  $I_2(A'^3\Pi_{2u})$  intermediate is attractive if we ignore the spectroscopic evidence for a  $T_e > 10,000 \text{ cm}^{-1}$ . This state must be collisionally and optically metastable if the sequential path ( $k_5$ ,  $k_8$ ) is followed. Vibrationally excited  $I_2$  is somewhat more tangible as an intermediate by means of sequential path ( $k_7$ ,  $k_6$ ), because  $I^*$  is known to be rapidly quenched by  $I_2$ . When we have made the assumption that this quenching process produces  $I_2^*$ , however, we are forced to conclude that  $k_6$  can compete against vibrational relaxation. The fact that  $t_{1/2}$  is independent of  $[Ar]$  is troubling.

Despite these ambiguities regarding  $I_2^*$ , the value of the analytic model lies in identifying the parameters that permit one to model the  $I_2$  dissociation data. The wall recombination rate,  $k_{13}$ , is necessary for understanding

the flow tube, although  $K_{SQ}(2) [\equiv (k_5k_8 + k_6k_7)/R_{I^{\ddagger}}]$  and the initiation terms  $k_{1a}$  and  $K_{SQ}(1) [\equiv k_5k_6/R_{I^{\ddagger}}]$  are the variables that ultimately control the production of I atoms in <sup>2</sup>the continuous-wave transfer laser. The results reported here are presented as constraints on a final set of rate coefficients employed to provide accurate numerical modeling. The rate coefficients given in Table 5 satisfy those constraints and are useful for modeling. Only more detailed experiments can identify  $I_2^{\ddagger}$  and provide a unique set of rate coefficients for the dissociation kinetics of  $I_2$  in electronically excited  $O_2$ .

# REFERENCES

1. S. J. Arnold, N. Finlayson, and E. A. Ogryzlo, J. Chem. Phys. 44, 2529 (1966).
2. R. G. Derwent and B. A. Thrush, Trans. Faraday Soc. 67, 2036 (1971).
3. R. G. Derwent and B. A. Thrush, Disc. Faraday Soc. 53, 162 (1972).
4. R. F. Heidner III, C. E. Gardner, T. M. El-Sayed, G. I. Segal, and J. V. V. Kasper, J. Chem. Phys. 74, 5618 (1981).
5. W. E. McDermott, N. R. Pchelkin, D. J. Benard, and R. R. Bousek, Appl. Phys. Lett. 32, 469 (1978).
6. D. J. Benard, W. E. McDermott, N. R. Pchelkin, and R. R. Bousek, Appl. Phys. Lett. 34, 40 (1979).
7. R. J. Richardson and C. E. Wiswall, Appl. Phys. Lett. 35, 138 (1979).
8. R. G. Derwent, D. R. Kearns, and B. A. Thrush, Chem. Phys. Lett. 6, 115 (1970).
9. R. G. Derwent and B. A. Thrush, Chem. Phys. Lett. 9, 591 (1971).
10. R. G. Derwent and B. A. Thrush, J. Chem. Soc. Faraday II, 68, 720 (1972).
11. R. G. Aviles, D. F. Muller, and P. L. Houston, Appl. Phys. Lett. 37, 358 (1980).
12. D. F. Muller, R. H. Young, P. L. Houston, and J. R. Wiesenfeld, Appl. Phys. Lett. 38, 404 (1981).
13. R. F. Shea, private communication.
14. R. F. Heidner III, C. E. Gardner, T. M. El-Sayed, and G. I. Segal, Chem. Phys. Lett. 81, 142 (1981).
15. R. F. Heidner III, Spectroscopic Properties of the  $O_2^* - I_2$  Flame, TR-0082(2610)-1, The Aerospace Corporation, El Segundo, California (to be published).
16. S. J. Davis and P. D. Whitefield, to be published.
17. D. St. A. G. Radlein, J. C. Whitehead, and R. Grice, Mol. Phys. 29, 1813 (1975).

18. E. B. Turner, G. Emanuel, and R. L. Wilkins, The NEST Chemistry Computer Program, TR-0059(6240-20)-1, The Aerospace Corporation, El Segundo, California, 1970.
19. J. Tellinghuisen and K. Wieland, J. Mol. Spectrosc, to be published.
20. G. Black, private communication (1980).
21. P. L. Houston, private communication (1981).
22. J. B. Koffend, R. Bacis, and A. Sebail, to be published (1982).
23. J. B. Koffend, F. J. Wodarczyk, R. Bacis, and R. W. Field, J. Chem. Phys. 72, 478 (1980).
24. A. T. Pritt, Jr., private communication (1982).
25. J. J. Deakin and D. Husain, J. C. S. Faraday II, 68, 41 (1972).
26. D. H. Burde and R. A. MacFarlane, J. Chem. Phys. 64, 1850 (1976).
27. A. J. Grimley and P. L. Houston, J. Chem. Phys. 68, 3366 (1978).
28. H. Hofmann, and S. R. Leone, J. Chem. Phys. 69, 641 (1972).



## APPENDIX A. DEFINITIONS FOR ANALYTIC MODELING

### I. Iodine Mass Balance

If the steady-state concentration of intermediate  $I_2$  states ( $I_2^*$ ) is small compared to  $[I_2]_0$ , iodine mass balance can be approximated as follows:

$$[I_2] = [I_2]_0 - 1/2 ([I] + [I^*]) \quad (A1)$$

Earlier work has established that Process (4) produces a rapid equilibrium between  $I(^2P_{1/2}, ^2P_{3/2})$  and  $O_2(^1\Delta, ^3\Sigma)$ , and we can write

$$[I^*]/[I] = K_{EQ} [I_\Delta]/[^3\Sigma] \equiv X \quad (A2)$$

The equilibrium constant,  $K_{EQ} \equiv k_4/k_{-4}$ , is 2.9 at  $T = 295$  K. Equations (A1) and (A2) can be combined to yield

$$[I^*] = \left( \frac{2X}{1+X} \right) ([I_2]_0 - [I_2]) \quad (A3)$$

Within that context,  $d[I^*]/dt = -[2X/(1+X)] d[I_2]/dt$ .

### II. $O_2(^1\Sigma)$ Behavior

As developed in Ref. 4, the steady-state concentration of  $O_2(^1\Sigma)$  can be represented in the general case (with  $I$ ,  $I^*$ , and  $I_2$  present) as

$$[^1\Sigma]_{ss} = \frac{(k_2 + k_3 [I^*]/[I_\Delta]) [I_\Delta]^2}{R_z} \quad (A4)$$

where  $R_I = k_9 [H_2O] + k_1 [I_2]_{ss} + k_{10}$ . In the dissociation region where  $[I_2]$  is changing rapidly, analysis is simplified if  $k_9[H_2O] + k_{10} \gg k_1[I_2]$ .

### III. Quenching of $I_2^{\ddagger}$

$$R_{I_2^{\ddagger}}(\text{sec}^{-1}) = k_6 [^1\Delta] + k_{-5} [^3\Sigma] + k_8 [I^*] + k_{-7} [I]$$

$$+ k_{11a} [H_2O] + k_{11b} [^3\Sigma] + k_{11c} [Ar] + k_{12} \quad (A5)$$

### IV. Steady-State Concentration of $I_2^{\ddagger}$

$$[I_2^{\ddagger}]_{ss} = \frac{(k_5 [^1\Delta] + k_7 [I^*]) [I_2(x)]}{R_{I_2^{\ddagger}}} \quad (A6)$$

APPENDIX B. ANALYTIC DISSOCIATION MODEL FOR  $I_2$   
INCLUDING I ATOM RECOMBINATION

The introduction of the wall recombination Process (13) into the kinetic scheme requires that the differential Eq. (16) be modified in the following manner:

$$\frac{-d [I_2]}{dt} = a [I_2] - b [I_2]^2 - d \quad (B1)$$

where

$$a = a_L + a_{SQ} + k_{13}$$

$$b = b_L + b_{SQ}$$

$$d = k_{13} [I_2]_0$$

The solution of this equation is given by Eq. (B2):

$$\frac{(2b [I_2] - a - \sqrt{-Q})}{(2b [I_2] - a + \sqrt{-Q})} \frac{(2b [I_2]_0 - a + \sqrt{-Q})}{(2b [I_2]_0 - a - \sqrt{-Q})} = \exp (\sqrt{-Q} t) \quad (B2)$$

where  $Q = 4bd - a^2$ . The following definitions are then useful:

$$\alpha = \frac{-a - \sqrt{-Q}}{2b}$$

$$\beta = \frac{-a + \sqrt{-Q}}{2b}$$

$$\gamma = ([I_2]_0 + \alpha) / ([I_2]_0 + \beta)$$

Using these definitions, the time dependent expression for  $[I_2]$  can be written

$$[I_2] = \frac{-\alpha + \beta \gamma \exp(\sqrt{-Q} t)}{(1 - \gamma \exp(\sqrt{-Q} t))} \quad (B3)$$

Unlike the result in Eq. (18), there is residual  $I_2$  at long times

$$[I_2]_{\infty} = -\beta \quad (B4)$$

A very useful approximation holds if  $[I]_0 = 0$  and  $a_{SQ} + a_c > k_{13}$ :

$$[I_2]_{\infty} \approx k_{13}/b \quad (B5)$$

We have chosen to define a dissociation time representing the time necessary to produce one-half of the total  $I$  atoms present at  $t = \infty$ . This definition is equivalent to the time necessary to reach the mean of the initial and final  $I_2$  concentrations:

$$[I_2]_{\text{mean}} = \frac{[I_2]_0 + [I_2]_{\infty}}{2} \quad (B6)$$

A half-life for dissociation within that context is:

$$t_{1/2} = \ln \left\{ \frac{[I_2]_0 + 2\alpha - \beta}{\gamma([I_2]_0 + \beta)} \right\} / \sqrt{-Q}$$

#### LABORATORY OPERATIONS

The Laboratory Operations of The Aerospace Corporation is conducting experimental and theoretical investigations necessary for the evaluation and application of scientific advances to new military space systems. Versatility and flexibility have been developed to a high degree by the laboratory personnel in dealing with the many problems encountered in the nation's rapidly developing space systems. Expertise in the latest scientific developments is vital to the accomplishment of tasks related to these problems. The laboratories that contribute to this research are:

Aerophysics Laboratory: Launch vehicle and reentry aerodynamics and heat transfer; propulsion chemistry and fluid mechanics; structural mechanics; flight dynamics; high-temperature thermomechanics; gas kinetics and radiation; research in environmental chemistry and contamination; cw and pulsed chemical laser development including chemical kinetics, spectroscopy, optical resonators and beam pointing; atmospheric propagation; laser effects and countermeasures.

Chemistry and Physics Laboratory: Atmospheric chemical reactions; atmospheric optics; light scattering; state-specific chemical reactions and radiation transport in rocket plumes; applied laser spectroscopy; laser chemistry; battery electrochemistry; space vacuum and radiation effects on materials; lubrication and surface phenomena; thermionic emission; photosensitive materials and detectors; atomic frequency standards; and bioenvironmental research and monitoring.

Electronics Research Laboratory: Microelectronics; GaAs low-noise and power devices; semiconductor lasers; electromagnetic and optical propagation phenomena; quantum electronics; laser communications; lidar; and electro-optics; communication sciences; applied electronics; semiconductor crystal and device physics; radiometric imaging; millimeter-wave and microwave technology.

Information Sciences Research Office: Program verification; program translation; performance-sensitive system design; distributed architectures for spaceborne computers; fault-tolerant computer systems; artificial intelligence; and microelectronics applications.

Materials Sciences Laboratory: Development of new materials: metal matrix composites, polymers, and new forms of carbon; component failure analysis and reliability; fracture mechanics and stress corrosion; evaluation of materials in space environment; materials performance in space transportation systems; analysis of systems vulnerability and survivability in enemy-induced environments.

Space Sciences Laboratory: Atmospheric and ionospheric physics; radiation from the atmosphere; density and composition of the upper atmosphere, aurora and airglow; magnetospheric physics; cosmic rays; generation and propagation of plasma waves in the magnetosphere; solar physics; infrared astronomy; the effects of nuclear explosions; magnetic storms; and solar activity on the earth's atmosphere, ionosphere, and magnetosphere; the effects of optical, electromagnetic, and particulate radiations in space or space systems.

END